CHALMERS
UNIVERSITY OF TECHNOLOGY

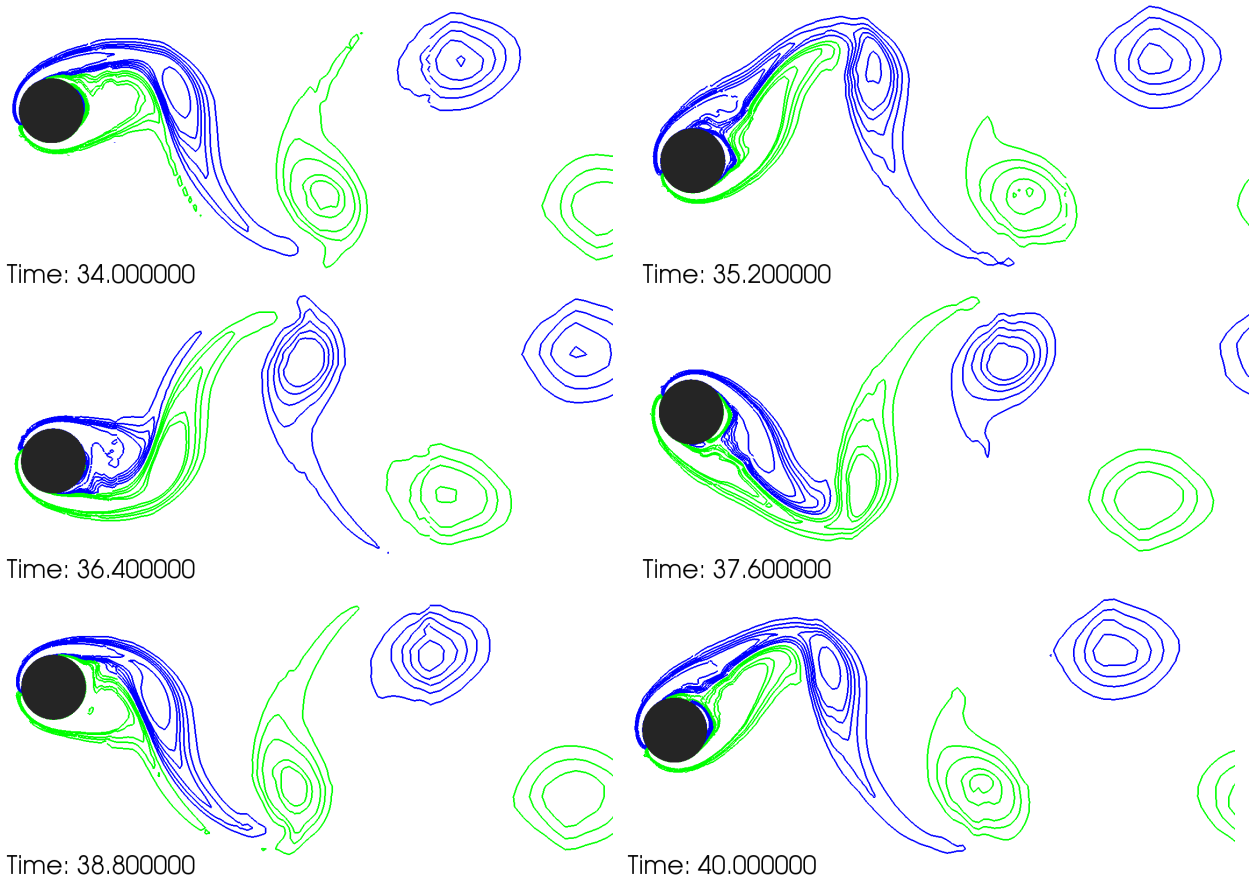

Coupling Algorithms for Fluid Structure Interaction at Low Density Ratios

Accuracy and Stability Analysis of Weak Coupling Algorithms in Partioned Codes

Master's thesis in Applied Mechanics

Martin Ottosson

Department of Mechanics and Maritime Science
CHALMERS UNIVERSITY OF TECHNOLOGY
Gothenburg, Sweden 2018

Master's thesis 2018:38

Coupling Algorithms for Fluid Structure Interaction at Low Density Ratios

Accuracy and Stability Analysis of Weak Coupling Algorithms in Partioned Codes

Martin Ottosson

CHALMERS
UNIVERSITY OF TECHNOLOGY

Department of Mechanics and Maritime Science
Division of Fluid Dynamics
Chalmers University of Technology
Gothenburg, Sweden 2018

Coupling Algorithms for Fluid Structure Interaction at Low Density Ratios
Accuracy and Stability Analysis of Weak Coupling Algorithms in Partioned Codes
Martin Ottosson

Supervisor: Andreas Mark and Christoffer Cromvik, Fraunhofer-Chalmers Centre
Examiner: Srdjan Sasic, Mechanics and Maritime Science

Master's Thesis 2018:38
Department of Mechanics and Maritime Science
Division of Fluid Dyhnamics
Chalmers University of Technology
SE-412 96 Gothenburg
Telephone +46 31 772 1000

Cover: *Countours of the instantaneous vorticity of an elastically mounted cylinder with $\rho = 4/\pi$ during approximately one period. (—) indicates negative vorticity while (—) indicates positive vorticity.*

Typeset in LaTeX
Gothenburg, Sweden 2018

Coupling Algorithms for Fluid Structure Interaction at Low Density Ratios
Accuracy and Stability Analysis of Weak Coupling Algorithms in Partioned Codes
Martin Ottosson
Department of Mechanics and Maritime Science
Chalmers University of Technology

Abstract

In recent years the interest of numerical predictions of fluid-structure interaction has grown in industrial applications as well as in the research of the phenomenon due to the increase in computational power. Numerical predictions of fluid-structure interaction typically suffers from instability when the solid-to-fluid density ratio becomes small. The instability issues are most severe when weak coupling, without coupling iterations within each time step, methods are used. Further, the weak coupling introduces the so-called artificial added mass effect, that introduces an error in the coupling.

At Fraunhofer-Chalmers Centre a state-of-the-art multiphase solver, IBOFlow, and a structural solver, LaStFEM, are developed. IBOFlow handles moving boundaries using the mirroring immersed boundary method with adaptive grid refinements. The incompressible Navier-Stokes equations together with the boundary conditions at the structural interface are solved on a Eulerian grid using the finite volume method. LaStFEM solves the structural equations together with the forces acting on the structural interface on a Lagrangian grid using the finite element method. In previous work, a strong coupling, with coupling iterations within each time step, and a simple weak coupling procedure has been implemented and validated.

In this thesis different weak coupling procedures are implemented, compared and analyzed in the existing frame work. The accuracy and stability of the weak coupling algorithms are investigated and compared to the existing strong coupling procedure. The investigation is done by the usage of three benchmarking cases: A rigid sphere attached to an undamped spring in Stokes flow, a rigid cylinder attached to a damped spring in a laminar flow and an elastic beam attached to a rigid cylinder in a laminar flow. The temporal and spatial accuracy are both found to be of second-order. The lowest solid-to-fluid density ratio where a stable solution was achived using a weak coupling algorithm is well below one and much smaller than what has been found in the literature.

Keywords: Fluid structure interaction, FSI Benchmark, Weak coupling method, Partitioned approach, Low density ratio, Immersed boundary method.

Acknowledgements

I would like to express my gratitude towards the following people for their support during my work:

Firstly I would like to thank my supervisors Andreas Mark and Christoffer Chromvik. Thank you Andreas for all help, interesting discussions, guidance in the work and the patience. The guidance in choosing suitable matrix solvers, methods and discretization schemes for the fluid solver has been very appreciated. Thank you Christoffer for your guidance in the existing fluid structure interaction framework, help with implementation and discussions about the structural solver. The colleagues at FCC are also acknowledged for great inspiration, a developing and pleasant working environment, especially Anders Ålund for all the help and with providing me with more computational power during the work. I would also like to extend a thank you to my examiner Srdjan Sasic.

Lastly, Thank you Martina Ståhl for all your patience and support!

Martin Ottosson, Gothenburg, June 2018

Contents

List of Figures

List of Tables

1
Introduction

This chapter will introduce the studied subject and give some motivations why it is of interest to study this phenomenon using computational tools.

1.1 Background

Fraunhofer-Chalmers Research Centre (FCC) develops computational tools for solving demanding industrial problems. At the department of Computational Engineering and Design a multiphase flow solver, IBOFlow [1], and a structural solver, LaStFEM, have been developed. IBOFlow efficiently handles moving boundaries using the mirroring immersed boundary method with adaptive grid refinements.

1.1.1 Fluid Structure Interaction

Fluid Structure Interaction (FSI) is a phenomenon which occurs in all systems where both a fluid and one, or multiple, structures are present. In many cases the structural deformation does not affect the overall system that is being studied and can therefore be neglected. In other cases it may be the driving mechanism and is therefore of great interest to study.

For most FSI problems an analytic solution to the governing equations cannot be derived due to the multidisciplinary and nonlinear nature of the phenomenon. Hence, the investigation of the phenomenon is limited to either laboratory experiments or numerical simulations. Accurate numerical simulations are in many cases superior to laboratory experiments in terms of understanding, optimization and economy. If the phenomenon is to be understood in detail the only option is numerical simulation since laboratory experiments always are limited in terms of what details that can be studied. The use of numerical simulations enables a greater possibility for optimization of both processes and products. Efficient numerical algorithms decreases the need for physical testing which reduces both costs and time for development.

With increasing computational capability it has in recent years become possible to solve complex and nonlinear mathematical problems to improve processes, improve functionality of products and understand different phenomena. Computation of systems which include FSI have become the subject of interest for a wide range of applications such as aircrafts [2, 3], wind turbines[4, 5], tall buildings [6], bridges[7], sloshing tanks [8] and various biomechanical applications [9] (Blod flow through the

compliant arteries [10], human vocal folds [11], flying [12] and swimming [13]) .

FCC has previously implemented and validated a framework for FSI where the flow solver, IBOFlow, and the structural solver, LaStFEM, have been coupled [14, 15].

1.1.2 Hemming

Hemming is a frequently used joining procedure in todays industry. Traditionally, welding has been the given joining method in industry. But as the demand on lighter weight grows, alternative methods must be used. Hemming enables the joining of different materials, which is needed in order to reach the demand on lighter weight. Currently the design of the hemming process is cumbersome since the process parameters are based on empirical formulas, experience and trial and error during laboratory experiments. Hence it is desirable to make more accurate predictions of the process parameters using computational tools. During hemming, an adhesive is squeezed between deformable parts, which creates both thin channels and multiple cavities. The process creates large fluid forces and the final deformation of the structure is highly dependant on the adhesive, meaning that the fluid and the structure is heavily coupled. At FCC the process has previously been studied using numerical simulations in cooperation with industrial manufacturing companies. One way coupled simulations, where the fluid forces acting on the structure interface is neglected, has successfully been performed. But due to the strong coupling, the two-way coupled simulations have become unstable. It is therefore of interest to implement and investigate the stability of different coupling algorithms.

1.2 Aim

The aim of this thesis is to review previous work within the area of fluid structure interaction and implement and analyze the stability and accuracy of different coupling methods.

1.3 Structure of Report

Following this introduction some basic theory is given in the next section. In the Methodology the methodology of both IBOFlow and LaStFEM is given and followed by the used coupling methods. The chapter is finished with a short description of the criterion when choosing suitable benchmarking cases and the approach for the stability analysis. The results are presented and discussed in chapter 4. Finally the thesis is concluded and recommended future work is discussed.

2
Theory

In the following chapter the theory used in this thesis is described.

2.1 Fluid Dynamics

In this section, a brief introduction to the basics of fluid dynamics and the numerical approaches used in this project is given.

2.1.1 Governing Equations

When studying a fluid, which can be observed as a continuum, the motion is governed by conservation equations. The governing equations are conservation of mass, conservation of momentum and conservation of energy. For a flow that can be considered as incompressible, meaning that the density remain constant, the equation of conservation of mass and conservation of momentum becomes decoupled from the conservation of energy.

For an incombressible flow the equation for conservation of mass is given by

$$\frac{\partial u_i}{\partial x_i} = 0 \tag{2.1}$$

and the equation for conservation of momentum is given by

$$\rho \frac{\partial u_i}{\partial t} + \rho u_j \frac{\partial u_i}{\partial x_j} = -\frac{\partial p}{\partial x_i} + \frac{\partial \tau_{ij}}{\partial x_j} + \rho g_i. \tag{2.2}$$

For a Newtonian fluid, the stress tensor, τ_{ij}, becomes

$$\tau_{ij} = \mu \left(\frac{\partial u_i}{\partial x_j} + \frac{\partial u_j}{\partial x_i} \right). \tag{2.3}$$

2.1.2 Handling of Arbitrary Boundaries

In fluid dynamics there exists two major approaches when dealing with arbitrary boundaries. The most common one is the conforming mesh method. Using this approach yields a more straightforward method regarding implementation of the boundary conditions. The drawback is that a new spatial discretization needs to be constructed each time a boundary moves or deforms which is computationally

expensive [16]. It exists several methods to decrease the computational cost when generating a new spatial discretization. But a common problem for all of them is that at big boundary movements, badly shaped cells are created which can undermine both the accuracy and stability of the solution. Even if an efficient and stable algorithm would be developed for handling the deformation of the spatial discretization there would still exist problems for colliding boundaries.

The other approach is so called non-conforming mesh methods. Using this approach is not as computationally expensive as a conforming mesh method regarding mesh generation, since there is no need for remeshing. Since there is no need for remeshing the method is more efficient and stable for a wide variety of problems. The drawback is that setting the boundary conditions is not as straight forward as for the conforming mesh methods. There exist several methods to enforce the boundary conditions at the correct position. Figure 2.1 shows an example of a problem discretized using either a conforming mesh method or non-conforming mesh method.

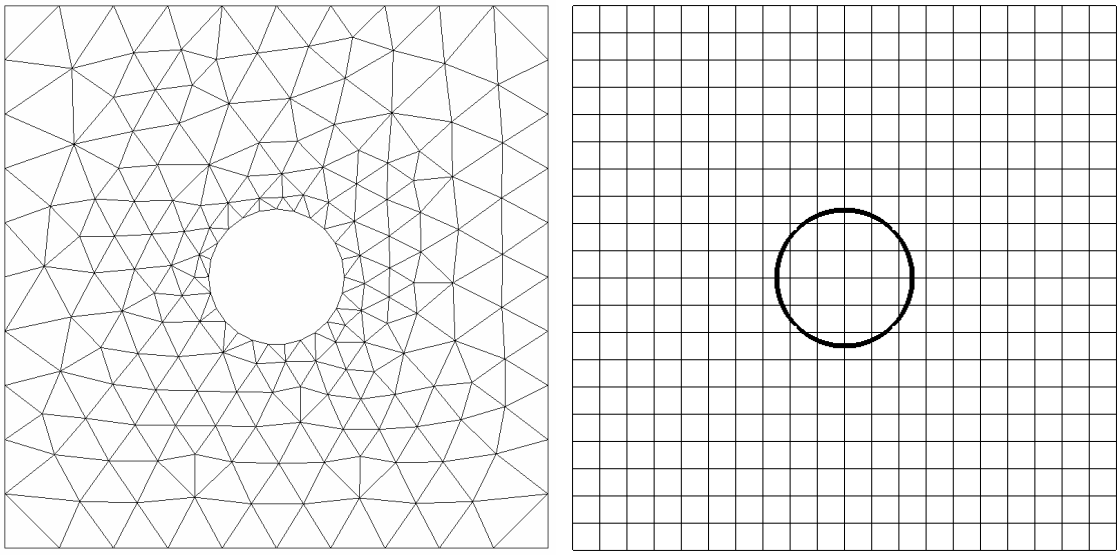

(a) *Conforming mesh.* **(b)** *Non-conforming mesh.*

Figure 2.1: *Example of a conforming mesh and a non-conforming mesh.*

The most common approach for non-conforming mesh methods are immersed boundary methods, in which a regular Eulerian grid is used for the fluid flow and a Lagrangian grid to represent the boundary. Immersed boundary methods can be divided into distributive methods and non-distributive methods. The distributive methods employ an external Lagrangian force in the presence of a boundary which is distributed onto the Eulerian grid over several cells. Since the representation of a boundary is distributed over several cells the interface of the boundary gets smeared. Hence, the non-distrubutive methods were developed where the boundary condition is enforced either via an external force. Derived from the momentum equation which ensures that the velocity at the location of the interface is the same for the fluid as for the immersed boundary or via an implicitly formulated boundary condition.

Originally the distributive Immersed Boundary Method were proposed by Peskin [17] where it was used to simulate the flow in a heart valve. The method used a discrete delta function to distribute the Lagrangian force onto the Eulerian grid in the presence of an immersed boundary. Since the Lagrangian force is distributed over several cells on the Eulerian grid, a large number of computational cells near the boundaries where needed in order to get a somewhat accurate representation of the interface. The proposed method was first-order accurate. Later Lai and Peskin [18] proposed an improved version of the method where the numerical diffusion was reduced and therefore performed better at higher Reynolds numbers. The distributive Immersed Boundary Method has since it where originally proposed been developed in several fashions to fit different problems. What is common for all of them is that the interface of the boundary is smeared out.

In order to remedy this problem, Mohd-Yousof [19] proposed a non-distributive approach where a force was introduced into the momentum equations in the presence of a immersed boundary. This approach ensures a correct boundary condition exactly at the location of the interface. The approach has further been investigated in [20], [21] and [22]. But since the method creates a fictitious reversed velocity field inside the immersed body instabilities issues was encountered since fluxes over the interface exists and the continuity equation cannot be fulfilled. Kim [23][24] introduced a new term into the continuity equation in order to ensure that continuity was fulfilled. The method has been validated and good agreement with previous results where obtained. The momentum forcing method, developed in [19], where extended to a boundary condition on the velocity by Majumdar and co-workers in [25]. Tseng and co-workers [26] developed a ghost-cell immersed boundary method which extrapolates the velocity on a point inside the IB in order to constrain the velocity at the immersed boundary. Both of these methods showed promising results but a nonphysical massflux over the interface is generated which causes oscillations in the solution.

Mark [16] developed an non-distributive immersed boundary method which exactly fulfills the velocity boundary condition at the interface of the immersed body and do not sacrifice mass continuity. The method is called The Mirroring Immersed Boundary Method. The method creates a fictitious velocity field inside the immersed boundary. The boundary condition may be written as

$$\frac{\mathbf{u}_{iib} + \mathbf{u}_e}{2} = \mathbf{u}_{ib} \tag{2.4}$$

where $\mathbf{u}_{ib}$ is the velocity at a point on the immersed boundary, $\mathbf{u}_e$ is a velocity outside of the immersed body in a point normal to the surface of the point on the immersed boundary and $\mathbf{u}_{iib}$ is the velocity inside of the immersed body in a point normal to the surface of the point on the immersed boundary. The velocities inside the immersed body, in the fictitious velocity field, is excluded when discretizing the mass conservation equation and the pressure correction equation and hence it is

ensured that there is no mass fluxes over the immersed boundary. The method has been validated in [27, 28].

2.2 Structural Dynamics

The motion of a rigid body is governed by Newton's second law and Euler's rotation equations. If the rigid body is prohibited from rotating the governing equation of motion reads

$$\ddot{\mathbf{x}}_s m_s = \sum_i \mathbf{F}_i \tag{2.5}$$

where $\ddot{\mathbf{x}}_s$ is the acceleration of the rigid body, m_s is the mass of the rigid body and $\mathbf{F_i}$ is the forces acting on the rigid body.

A deformable body is modeled as an elastic continuum and the motion and deformation is governed by balance of linear momentum. The balance of linear momentum in a continuum point is given by

$$\nabla \cdot \sigma + \rho_s \mathbf{g} - \rho_s \ddot{\mathbf{x}}_s = \mathbf{0}, \tag{2.6}$$

where $\nabla\cdot$ is the divergence operator, σ is the Cauchy stress, ρ_s is the density of the object, $\mathbf{g}$ is the gravity force and $\ddot{\mathbf{x}}_s$ is the acceleration of the contiuum point.

2.3 Fluid Structure Interaction

Fluid Structure Interaction (FSI) problems can be solved using two different numerical approaches. One can either use a monolithic approach or a partitioned approach. With a monolithic approach the fluid and the structure are treated in the same mathematical framework. This forms a single system of equations, and therefore a single matrix, which can be solved in a single unified algorithm. In a partitioned approach the two fields are treated separately and has their own mathematical and numerical framework. The two fields communicate explicitly or semi implicitly.

A monolithic approach can potentially achieve a higher accuracy and better stability but since everything is done in a unified algorithm the code requires a great deal of expertise and resources. Using an monolithic approach forms a single matrix which contains all the unknown variables. Even for quite simple problems this matrix becomes very large and the off-diagonal terms, also called coupling terms, will vary in size. Due to the multidisciplinary nature of fluid structure problems, different solving algorithms are suited for the different part of the matrix. This causes a problem when developing an efficient solving algorithm for the system. Since all of the unknowns are treated in the same matrix the possibility of an ill-conditioned system also increases.

Using a partitioned approach requires less development since separate fluid and structural codes can be employed and the challenge instead becomes to develop a

suitable algorithm for how the information should be communicated between the two codes. Since existing approaches within each field can be used in a partitioned approach, state-of-the-art codes, modeling and numerical algorithms within each field can be used. Meaning that a successfully implemented partitioned FSI approach has greater potential when it comes to using sophisticated fluid and structure physics. The drawback of using a partitioned approach is to develop an efficient method for exchanging information between the two computational fields.[29]

2.3.1 Partitioned Approaches

When using a partitioned approach the idea is that the separate solvers for the fluid field and the structural movement is treated as "black-boxes". These approaches can be divided into two different classifications, strong coupling methods and weak coupling methods. Strong coupling methods are algorithms where equilibrium at each time step is ensured through coupling iterations, with or without under-relaxation. In contrast to strong coupling methods, in weak coupling methods the fluid field and the structural movement/deformation is only solved once in each time step. This greatly decreases the computational power needed when solving a problem. But since equilibrium is not enforced at each time step, weak coupling methods suffers from from a miss match in time and space and increased instability[30].

2.3.2 Literature Review

In the following section a selection of interesting work made within the area of FSI has been reviewed.

He and co-workers [31] developed a non-linear structural solver to couple with an existing flow solver based on a non-distributive immersed boundary method. Both a strong coupling and a weak coupling method were implemented and validated against an existing numerical benchmark case. The implemented procedures showed good agreement with previous results for both the strong and the weak coupling method. But as the solid-to-fluid density ratio decreased the weak coupling became unstable while the strong coupling procedure still gave a stable solution with good agreement compared to other studies. The weak coupling was performed by letting the fluid domain advance from time t to $t + \Delta t$ assuming that the interface is as calculated at time t. This was followed by calculating the forces acting on the structure from the fluid and solving the structural deformation/movement, which ends one time step. The strong coupling method were performed using Gauss-Seidel iterations between the flow solver and the structural solver without any under-relaxation of the structural displacement. The iterations were performed until the interface location did not change more than a specified criteria between the iterations.

In [32] Huang and Sung developed a distributive immersed boundary method which was coupled with a structural solver. They implemented a weak coupling method where the interface of the immersed boundary at the next time-step was estimated

as

$$\tilde{\mathbf{x}}^n = \mathbf{x}^{n-1} + \Delta t \dot{\mathbf{x}}^{n-1} \tag{2.7}$$

where $\tilde{\mathbf{x}}^n$ is the predicted position of the interface at time step n, $\mathbf{x}^{n-1}$ is the position and $\dot{\mathbf{x}}^{n-1}$ is the velocity of the interface at time step $n-1$ and Δt is the size of the time step. The method was validated against various biological cases and showed good agreement with previous studies. The temporal and spatial convergence rate was showed to be between first order and second order. The stability of the method was not investigated.

In order to increase the stability when using computationally efficient weak coupling methods Kim and Choi [33] proposed a new interface predictor method with a free parameter. The interface were predicted according to

$$\begin{aligned} \tilde{\dot{\mathbf{x}}}^n &= \dot{\mathbf{x}}^{n-1} + \Delta t \left(\xi \ddot{\mathbf{x}}^{n-1} + (1-\xi) \ddot{\mathbf{x}}^{n-2} \right), \\ \tilde{\mathbf{x}}^n &= \mathbf{x}^{n-1} + \Delta t \tilde{\dot{\mathbf{x}}}^n. \end{aligned} \tag{2.8}$$

The proposed weak coupling method was compared with a strong coupling based on Gauss-Seidel iterations together with Aitken under-relaxation of the interface motion. Both coupling methods showed good agreement with previous results and second-order spatial accuracy. Stable solutions for both methods were obtained for solid-to-fluid density ratios well below one. The weak coupling method became most stable when the free parameter were set to $\xi = 3/4$. The weak coupling method needed 4-7 times less computational time compared to the strong coupling method.

In [34] Dettmer and Peric proposed a new weak coupling method where the forces excerted on the structure by the fluid is predicted and underrelaxed over time instead of a prediction of the interface position, which is the most common approach. The proposed method can be divided into four parts

1. Predict fluid forces on the structure as

$$\tilde{\mathbf{F}}^n = 2\mathbf{F}^{n-1} - \mathbf{F}^{n-2} \tag{2.9}$$

   where $\mathbf{F}^{n-1}$ and $\mathbf{F}^{n-2}$ are the fluid forces from the previous time step.
2. Load structure with the predicted fluid force $\tilde{\mathbf{F}}^n$ and solve structural deformation/motion.
3. Solve fluid flow.
4. Average the fluid force as

$$\mathbf{F}^n = \beta \hat{\mathbf{F}}^n + (1-\beta)\tilde{\mathbf{F}}^n \tag{2.10}$$

   where $\hat{\mathbf{F}}^n$ is the actual force exerted by the fluid on the structure.

The proposed method showed good agreement with previous studies and by lowering β stability could be achieved. Setting β to a small value decreased the methods capability of capturing high frequencies. For some cases $\beta = 0.005$ was needed in order to achive stable solutions. It was concluded that the proposed method had the same range of applicability as a Gauss-Seidel method for the studied problems, but at a much lower computational cost.

Förster and co-workers [30] investigated the so-called artificial added mass effect which often is responsible for instability issues when conducting numerical simulation of fluid structure interaction in a incompressible flow using interface predictors. It was concluded that a decreasing solid-to-fluid density ratio increased the instability issues. Higher order schemes for both temporal discretization of the fluid domain and interface predictors, decreasing time step, increasing fluid viscosity and decreasing structural stiffness also had a negative effect on the stability. Three different interface predictors were studied. The zeroth order accurate is given by

$$\tilde{\dot{\mathbf{x}}}^n = \dot{\mathbf{x}}^{n-1}, \tag{2.11}$$

the first order is given by

$$\tilde{\mathbf{x}}^n = \mathbf{x}^{n-1} + \Delta t \dot{\mathbf{x}}^{n-1}, \tag{2.12}$$

and

$$\tilde{\mathbf{x}}^n = \mathbf{x}^{n-1} + \Delta t \left(\frac{3}{2} \dot{\mathbf{x}}^{n-1} - \frac{1}{2} \dot{\mathbf{x}}^{n-2} \right), \tag{2.13}$$

is a second order accurate interface predictor. It was concluded that all weak coupling methods become unstable at a certain density ratio. Hence, for problems which suffers from major instabilities a strong coupling need to be used in order to enforce stability. Even though the artificial added mass effect is most pronounced when using a weak coupling, strong coupling methods also suffer from instabilities due to this effect and a large number of iterations between the solvers may be needed to achieve stable solutions.

3
Methodology

In the following chapter the methods used in this thesis are explained.

3.1 Fluid Solver: IBOFlow

The fluid solver used in this project is an Immersed Boundary Octree multiphase Flow solver, IBOFlow, and is developed at Fraunhofer-Chalmers Centre. IBOFlow solves the governing equations on a co-located dynamic octree grid. In order to obtain the correct pressure the SIMPLEC [35] method is employed. To prevent decoupling of the pressure and velocity field, pressure weighted flux interpolation by Rhie and Chow [36] is used. Immersed objects are accounted for by using the mirroring immersed boundary method. IBOFlow has been previously used to study conjugated heat transfer [37] together with geometry optimization [38, 39]. In automotive industry the solver have been successfully used to efficiently simulate robot application of sealing material [40, 41], adhesives [42] and painting [43, 44, 45, 46, 47, 48]. A new emerging and interesting field is 3D bioprinting, where the solver has been used to predict the printability of nanofibrillar inks [49].

3.1.1 The Mirroring Immersed Boundary Method

The mirroring immersed boundary method is developed and validated in [28] by Mark and co-workers and creates a fictitious velocity field inside the immersed body in order to constrain the velocity to an exact value at the exact position of the immersed boundary. To ensure that no fluxes exists over the immersed boundary the fictitious velocity field is excluded from the continuity equation.

The method firstly determines if the cell centers lies outside the immersed boundary, inside and near the immersed boundary (IIB node) or far inside the immersed boundary. The IIB node is mirrored over the immersed boundary to create a fictitious point in the flow field. The velocity at the fictitious point in the flow field is determined as

$$\frac{\mathbf{u}_{iib} + \mathbf{u}_e}{2} = \mathbf{u}_{ib} \tag{3.1}$$

where $\mathbf{u}_{ib}$ is the velocity at a point on the immersed boundary, $\mathbf{u}_e$ is a velocity outside of the immersed body in the fictious exterior point and $\mathbf{u}_{iib}$ is the fictitious velocity in the IIB node. This is done for every IIB point. To determine the velocity in the actual nodes outside, but near the immersed boundary trilinear interpolation is used.

3.1.2 Calculation of the Surface Forces

IBOFlow is given the shape and position of the solid from LaStFEM each time the shape or position is updated. In IBOFlow geometries are represented as triangulated surfaces. Hence, LaStFEM creates a triangulation of surface and transfers it to IBOFlow. The total force, F_i is given by the surface integral of the stress tensor over the immersed boundary (IB) as

$$F_i = \int_{\mathrm{IB}} \left(-p\delta_{ij} - \mu_f \left(\frac{\partial u_i}{\partial x_j} + \frac{\partial u_j}{\partial x_i} \right) \right) n_j \mathrm{d}S. \tag{3.2}$$

The stress tensor,

$$\sigma = -p\delta_{ij} - \mu_f \left(\frac{\partial u_i}{\partial x_j} + \frac{\partial u_j}{\partial x_i} \right), \tag{3.3}$$

is calculated in the center of each triangle. This is done by trilinear interpolation from all surrounding exterior points. Interior points are excluded from the interpolation. The stress tensor, σ, is then integrated in each triangle and summation of the forces in all triangles yields the total surface force.

3.1.3 Convective and Time Schemes

The choice of convective scheme is important in terms of stability and accuracy. A lower order scheme usually yields better stability but also causes numerical diffusion. The convective scheme is used to discretize the convective terms ($\partial/\partial x_i$) in the governing equations. For all studied cases in this thesis the ULTIMATE QUICKEST scheme developed in [50] hase been used.

For temporal discretization the implicit Euler scheme has been used.

3.2 Structural Solver: LaStFEM

3.2.1 Time scheme

The temporal discretization of the governing equation for a solid object is done with Newmark's time stepping scheme developed in [51]. The method reads

$$\begin{aligned} \dot{\mathbf{x}}_s^n &= \dot{\mathbf{x}}_s^{n-1} + \Delta t \left((1-\gamma)\ddot{\mathbf{x}}_s^{n-1} + \gamma \ddot{\mathbf{x}}_s^n \right) \\ \mathbf{x}_s^n &= \mathbf{x}_s^{n-1} + \Delta t \dot{\mathbf{x}}_s^{n-1} + \frac{1}{2}\Delta t^2 \left((1-2\beta)\ddot{\mathbf{x}}_s^{n-1} + 2\beta \ddot{\mathbf{x}}_s^n \right) \\ \gamma &\in [0,1] \quad \text{and} \quad \beta \in [0,1/2]. \end{aligned} \tag{3.4}$$

In structural dynamics it is often of interest to solve for the static deformation of an object. Meaning that the acceleration becomes zero. In these cases it is unpractical to solve for acceleration and therefore the governing equations are reformulated so that instead of primarily solving for acceleration, displacement is primarily solved

for. Hence, Newmark's time stepping scheme is rewritten as

$$\begin{aligned}\dot{\mathbf{x}}_s^n &= \frac{\gamma}{\beta\Delta t}\left(\mathbf{x}_s^n - \mathbf{x}_s^{n-1}\right) + \left(1 - \frac{\gamma}{\beta}\right)\dot{\mathbf{x}}_s^{n-1} + \Delta t\left(1 - \frac{\gamma}{2\beta}\right)\ddot{\mathbf{x}}_s^{n-1} \\ \ddot{\mathbf{x}}_s^n &= \frac{1}{\beta\Delta t^2}\left(\left(\mathbf{x}_s^n - \mathbf{x}_s^{n-1}\right) - \Delta t\dot{\mathbf{x}}_s^{n-1} - \Delta t^2(0.5-\beta)\ddot{\mathbf{x}}_s^{n-1}\right)\end{aligned} \tag{3.5}$$

The same choice of γ and β has been used through out the thesis and were chosen as

$$\begin{aligned}\gamma &= 0.5 \\ \beta &= 0.25\end{aligned} \tag{3.6}$$

known as the constant average acceleration method.

3.2.2 Elasticity model

The elasticity model used for deformable objects has been the St. Venant-Kirchoff hyperelastic material model. The model accounts for large deformations and the second Piola-Kirchoff stress is given by [52]

$$S = \lambda(tr(E))I + 2\mu E \tag{3.7}$$

where λ and μ are the Lamé constants, E is the Lagrangian Green strain and I is the second-order unit tensor. The relation between the Cauchy stress, σ, and the second Piola-Kirchoff stress, S, is given by

$$\sigma = J^{-1}F \cdot S \cdot F^T \tag{3.8}$$

where F is the deformation gradient and $J = \det F$. The Green strain, E, can be expressed as

$$E = \frac{1}{2}(F^T \cdot F - I) \tag{3.9}$$

3.3 Coupling Methods

In the following section the coupling methods used and investigated in this project are presented. A method used when coupling two separate solvers, which each solves a specific type of problem, is called a weak coupling method if each solver is used only once in each time step. Hence, equilibrium is not enforced at each time step. Due to this fact weak coupling method often suffer from instabilities. The aim when using a weak coupling method is to lower the computational cost needed to solve a problem at the cost of both accuracy and stability. In contrast to this, a strong coupling method iterates between the two different solvers until equilibrium is enforced at each time step.

3.3.1 Weak Coupling Methods

In this thesis the weak coupling methods implemented has been divided into three different categories. The categories are interface predicting methods, force predicting methods and force smoothing methods. Since all the weak coupling methods needs the same number of solutions for each separate solver the only difference in computational power needed is the difference which arise from the algebraic expressions within the algorithms. Hence, the difference in computational cost needed within different weak coupling methods are negligible. The most simple version of a weak coupling method is presented in algorithm 1 and will henceforth be called the explicit coupling.

Algorithm 1: *Explicit coupling method.*

At time step n

1. Advance fluid domain to time step n with the boundary condition at the interface of the structure as calculated at time step $n-1$.
2. Calculate the forces acting on the structural interface.
3. Advance structural domain to time step n.
4. Advance to next time step.

3.3.1.1 Interface Predicting Method

When using the interface predicting method the idea is to predict the position, velocity and acceleration of the structural interface at time step n depending on the state of the interface at previous time step. Hence, increasing the stability and accuracy of the numerical approach. The method is presented in algorithm 2.

Algorithm 2: *Interface predicting coupling method.*

At time step n

1. Predict position, velocity and acceleration of interface at time step n by using information from previous time steps.
2. Advance fluid domain to time step n with the boundary condition at the interface of the structure as predicted in 1.
3. Calculate the forces acting on the predicted structural interface.
4. Advance structural domain to time step n from time step $n-1$.
5. Advance to next time step.

The next step is to decide how the interface should be predicted. In this thesis three different approaches suggested in the literature has been used. The first is a simple first order predictor where one assumes that the velocity of the interface will

remain constant throughout the time step. The prediction is given by

$$\begin{aligned}\tilde{\ddot{\mathbf{x}}}^n &= \ddot{\mathbf{x}}^{n-1},\\ \tilde{\dot{\mathbf{x}}}^n &= \dot{\mathbf{x}}^{n-1},\\ \tilde{\mathbf{x}}^n &= \mathbf{x}^{n-1} + \Delta t\dot{\mathbf{x}}^{n-1}\end{aligned} \tag{3.10}$$

where the superscript indicates time step, $\dot{(\,)}$ indicates time derivative, $\mathbf{x}$ is the location of the interface and $\tilde{(\,)}$ indicates a predicted value. The second approach is a second order accurate predictor which accounts not only for the most recent time step but the two most recent time steps.

$$\begin{aligned}\tilde{\ddot{\mathbf{x}}}^n &= \ddot{\mathbf{x}}^{n-1},\\ \tilde{\dot{\mathbf{x}}}^n &= \frac{3}{2}\dot{\mathbf{x}}^{n-1} - \frac{1}{2}\dot{\mathbf{x}}^{n-2},\\ \tilde{\mathbf{x}}^n &= \mathbf{x}^{n-1} + \Delta t\tilde{\dot{\mathbf{x}}}^n.\end{aligned} \tag{3.11}$$

The third approach is also a second order accurate predictor but instead of predicting the velocity of the interface dependant on the previous time steps the acceleration of the interface is predicted. It may be written as

$$\begin{aligned}\tilde{\ddot{\mathbf{x}}}^n &= \xi\ddot{\mathbf{x}}^{n-1} + (1-\xi)\ddot{\mathbf{x}}^{n-2},\\ \tilde{\dot{\mathbf{x}}}^n &= \dot{\mathbf{x}}^{n-1} + \Delta t\tilde{\ddot{\mathbf{x}}}^n,\\ \tilde{\mathbf{x}}^n &= \mathbf{x}^{n-1} + \Delta t\tilde{\dot{\mathbf{x}}}^n.\end{aligned} \tag{3.12}$$

In [33] the effect on the stability of the free parameter ξ was investigated. It was found to achieve the best stability if the free parameter was set to $\xi = \frac{3}{4}$ and therefore this has been used in this thesis.

3.3.1.2 Force Predicting Method

The force predicting method may be seen in a similar way as the interface predictor methods. The idea is the same, that one may predict the behaviour of the structure dependant on previous time steps. But instead of predicting the position, velocity and acceleration of the interface the aim is to achieve a more accurate prediction and therefore better stability by predicting the forces acting on the structural interface. The method is shown in algorithm 3.

Algorithm 3: *Force predicting coupling method.*

At time step n

1. Predict the forces exerted on the structure by the fluid as

$$\tilde{\mathbf{F}}^n = 2\mathbf{F}^{n-1} - \mathbf{F}^{n-2} \tag{3.13}$$

   where $\mathbf{F}^{n-1}$ and $\mathbf{F}^{n-2}$ are the forces exerted on the structure by the fluid at previous time steps.
2. Advance structural domain to time step n from time step $n-1$ with the predicted force.
3. Advance fluid domain to time step n with the boundary condition at the interface of the structure as predicted in 2.
4. Calculate the forces acting on structural interface, $\hat{\mathbf{F}}^n$.
5. Filter the forces as

$$\mathbf{F}^n = \beta\hat{\mathbf{F}}^n + (1-\beta)\tilde{\mathbf{F}}^n \tag{3.14}$$

6. Advance to next time step.

The method have been proposed in [34] and which parameter β that was needed in order to a obtain stable solution was highly dependent on what case that were simulated. For some cases a $\beta = 0.005$ were needed. Decreasing β sacrifices the accuracy of the calculation in order to achieve stability.

3.3.1.3 Force Smoothing Method

As an outcome of this thesis a new coupling method for fluid structure interaction is proposed. The method is mainly inspired from the force predictor method. The idea is mainly to incorporate the filtering of forces exerted by the fluid on the structure into the explicit coupling since white noise in these forces has been found to often be the reason for instabilities. The method is shown in algorithm 4.

Algorithm 4: *Force smoothing coupling method.*

At time step n

1. Advance fluid domain to time step n with the boundary condition at the interface of the structure as calculated at time step $n-1$.
2. Calculate the forces acting on structural interface, $\hat{\mathbf{F}}^n$.
3. Filter the forces as

$$\mathbf{F}^n = \beta\hat{\mathbf{F}}^n + (1-\beta)\mathbf{F}^{n-1} \tag{3.15}$$

4. Advance structural domain to time step n by letting $\mathbf{F}^n$ act on the structural interface.
5. Advance to next time step.

By setting $\beta = 1$ the algorithm becomes identical with a explicit coupling and by setting $\beta = 0$ the influence of the fluid on the structure is completely neglected. Meaning that the the coupling can always be made stable by lowering β but at the

expense of accuracy. In problems where one only wants to study frequencies that are much bigger than the needed time step the procedure is suitable. But if a low enough β is used the simulation will not be able to capture the actual behaviour of the system.

3.3.2 Strong Coupling Method

To be able to determine the accuracy of the implemented weak coupling methods a reference solution is needed. This is achieved by using a strong coupling method which iterates between the two solvers within every time step until equilibrium is achieved. In this thesis a Gauss-Seidel method has been used. In order to increase the convergence rate Aitken[53] under relaxation of the structure has been used. The coupling method is shown in algorithm 5.

Algorithm 5: *Strong coupling method.*

At time step n

1. Let the structure remain at the same state as calculated at time step $n-1$.
2. Advance fluid domain to time step n.
3. Calculate the forces acting on the structural interface.
4. Advance structural domain to time step n in order to obtain intermediate displacement, $\hat{\mathbf{x}}^{n,k}$, velocity, $\hat{\dot{\mathbf{x}}}^{n,k}$, and acceleration, $\hat{\ddot{\mathbf{x}}}^{n,k}$, where k is the iteration index.
5. Under relax the structure motion using Aitken under relaxation as

$$\mathbf{x}^{n,k} = \mathbf{x}^{n,k-1} + \omega^{n,k}\left(\hat{\mathbf{x}}^{n,k} - \mathbf{x}^{n,k-1}\right) \tag{3.16}$$

where the under-relaxation factor at the kth iteration, $\omega^{n,k}$, for $k \geq 2$ is given by

$$\omega^{n,k} = -\omega^{n,k-1}\frac{\left(\hat{\mathbf{x}}^{n,k-1} - \mathbf{x}^{n,k-2}\right)^T\left(\left(\hat{\mathbf{x}}^{n,k} - \mathbf{x}^{n,k-1}\right) - \left(\hat{\mathbf{x}}^{n,k-1} - \mathbf{x}^{n,k-2}\right)\right)}{\left|\left(\hat{\mathbf{x}}^{n,k} - \mathbf{x}^{n,k-1}\right) - \left(\hat{\mathbf{x}}^{n,k-1} - \mathbf{x}^{n,k-2}\right)\right|^2} \tag{3.17}$$

and

$$\mathbf{x}^{n,0} = \mathbf{x}^{n-1}, \quad \dot{\mathbf{x}}^{n,0} = \dot{\mathbf{x}}^{n-1}, \quad \ddot{\mathbf{x}}^{n,0} = \ddot{\mathbf{x}}^{n-1} \quad \text{and} \quad \omega^{n,1} = \max\left(\omega^{n-1}, 1\right) \tag{3.18}$$

6. Check convergence:

$$\begin{aligned} &\text{if} \quad \frac{R_i}{R_0} \geq \varepsilon \quad \text{Go back to step 2} \\ &\text{if} \quad \frac{R_i}{R_0} < \varepsilon \quad \text{Proceed to step 7} \end{aligned} \tag{3.19}$$

where the sub index indicates iteration.

7. Advance to next time step.

The residual, R_i, is calculated by taking the relative off balance from the governing

equations. Meaning that how it is defined is different from a rigid body compared to an elastic body. For a rigid body the residual is calculated as

$$R_i = \sum_{k=1}^{3} |\ddot{\mathbf{x}}_{s,k}^{i} m_s - \sum_{j} \mathbf{F}_{j,k}^{i}| \tag{3.20}$$

and for a elastic body the residual is calculated as in a similar manner, but as a balance of the internal and the external forces over all nodes.

The method is well known within the field of FSI and is often used for comparison when studying weak coupling methods. The implemented version has been validated in [14] and [15]. The method is superior to weak coupling methods in terms of stability but may increases the computational cost needed with several magnitudes[34]. It exist several quasi-Newton methods within the literature which has been proven superior to this method in both terms of computational power needed and stability but those have not been the focus of this thesis.

3.4 Benchmarking Cases

When implementing new methods into an existing code it is important to use well designed benchmarking cases to validate and investigate the robustness of the method. The cases should be demanding in terms of the part of the code that one is interested in and not "push" the rest of the code to the limit. Therefore the validation cases chosen in this thesis does not include complex flow fields or demanding structural motion or deformation. All of the cases occur at rather low Reynolds numbers and is therefore laminar and no complex turbulence models are needed. The fluid in all cases are a single phase fluid. Regarding the structural solver the idea has been to gradually increase the complexity from rigid objects to deformable objects since the implementation in the code regarding the two differ. It is also important that the case has been used to validate several other codes in order to deem what may be seen as an accurate result when solving this problem and to exclude the possibility that the published result may not be accurate.

In the present thesis the first benchmarking case has been a rigid body immersed in a low Reynolds number flow. For this case an analytic solution exist which the numerical solution can be compared to. The second case still consists of a rigid body immersed in a laminar flow but at a higher Reynolds number, where a analytic solution do not exist. Due to the higher Reynolds number the behaviour of the system is transient and one can analyze the stability of different coupling algorithms. The third case consists of a deformable body immersed in a laminar flow which also creates an unsteady system.

3.5 Stability Analysis

As discussed in the theory chapter, decreasing solid-to-fluid density ratios increases instability issues when numerically solving fluid structure interaction problems. The stability analysis in this thesis has therefore been conducted by decreasing the solid-to-fluid density ratio until instability has been reached. This approach has been used in previous work by [33] and [30] among others.

4

Results and Discussion

In the following section the results from the project are presented and discussed. The implemented coupling methods have been validated and analyzed using three different cases.

4.1 Analytic Case: Rigid Sphere Attached to a Spring in Stokes Flow

To ensure that the implementation is correct it was tested against a case which has been solved analytically. The case consists of a rigid sphere in a three dimensional stokes flow, $Re \lesssim 1$, which is attached to an undamped spring. The case is solved using three different approaches. Firstly a analytic solution is derived. Secondly the problem is solved using different coupling methods in a one dimensional solver. Lastly the problem is solved using different coupling methods between the three-dimensional solvers IBOFlow and LaStFEM.

4.1.1 Parameters and Analytical Solution

The sphere is only allowed to move in the direction of the flow and the equation of motion therefore reads

$$m_s \ddot{x}_s = \sum F = F_{Drag} - F_{Spring}. \tag{4.1}$$

The spring force is determined by the spring constant k and the sphere's offset from its original position as

$$F_{spring} = k x_s. \tag{4.2}$$

Since Stokes flow is assumed, the drag force acting on the sphere can be determined analytically [54]. The expression for the drag force may be written as

$$F_{Drag} = 6\pi r_s \mu_f U_0 \tag{4.3}$$

where r_s is the radius of the sphere,μ_f is the dynamic viscosity and $U_0 = U - \dot{x}_s$ is the slip velocity which is the difference between the free stream velocity, U and the velocity of the sphere, $\dot{x}_s$. Inserting the expression of the spring force and the drag force into the equation of motion the governing equation for the system may be written as

$$\ddot{x}_s + \frac{6\pi r_s \mu_f}{m_s}\dot{x}_s + \frac{k}{m_s}x_s = \frac{6\pi r_s \mu_f U}{m_s} \tag{4.4}$$

Since it is of interest to study how well the implemented coupling algorithms perform compared to the analytic solution one want to create a moderate damped system. Meaning that the parameters should be chosen so that some initial oscillations occur before the steady state solution is reached. This may be done by setting criteria on the parameters so that the characteristic equation to the homogeneous part of the governing equation gives complex roots. The characteristic equation to the homogeneous part of the governing equation is given by

$$\lambda^2 + \frac{6\pi r_s \mu_f}{m_s}\lambda + \frac{k}{m_s} = 0. \tag{4.5}$$

The roots to this equation becomes

$$\lambda = -\frac{\frac{6\pi r_s \mu_f}{m_s}}{2} \pm \sqrt{\left(\frac{6\pi r_s \mu_f}{m_s}\right)^2 - \frac{k}{m_s}} \tag{4.6}$$

If the roots are to be complex then the criterion is given by

$$\left(\frac{6\pi r_s \mu_f}{m_s}\right)^2 - \frac{k}{m_s} < 0 \quad \Rightarrow \quad \frac{27\pi\mu_f^2}{4\rho_s r_s} < k \tag{4.7}$$

Before one proceeds, lets recall that Stoke's flow has been assumed. Meaning that it also exists a restriction on the Reynolds number

$$Re = \frac{\rho_f U_0 2r_s}{\mu_f} \approx \frac{\rho_f U 2r_s}{\mu_f} \lesssim 1. \tag{4.8}$$

Lets choose the parameters to be

$$Re = 0.1, \quad U = 1, \quad \rho_f = 1, \quad \rho_s = 300 \quad \text{and} \quad r = 0.5. \tag{4.9}$$

Which leads to

$$\mu_f = 10 \quad \text{and} \quad k > 4.5\pi. \tag{4.10}$$

Through some trial and error $k = 300$ were deemed to give an desirable behaviour. A summation of the choosen parameters is given in table 4.1.

Table 4.1: *Used parameters for the elastically mounted sphere.*

Re[1]	U[m/s]	μ_f [kg/ms]	ρ_f[kg/m^3]	ρ_s[kg/m^3]	r_s [m]	k [N/m]
0.10	1.00	10.0	1.00	300	0.50	300

Lets separate the roots into the real part and the imaginary part as

$$\lambda = a \pm bi \tag{4.11}$$

the analytic solution to the problem may be written as

$$x_s(t) = C_1 e^{at}\cos bt + C_2 e^{at}\sin bt + \frac{6\pi r_s \mu_f U}{k}. \tag{4.12}$$

The sphere is starting from rest, $x_s(t=0) = 0$ m and $\dot{x}_s(t=0) = 0$ m/s, meaning that the constants in the expression becomes

$$C_1 = -\frac{6\pi r_s \mu_f U}{k} \quad \text{and} \quad C_2 = -C_1 \frac{a}{b} \tag{4.13}$$

The analytic solution is shown in figure 4.1. The sphere behaves as expected. Some oscillations occurs before it reaches steady state and by studying the expression of the drag coefficient,

$$C_D = \frac{2F_{Drag}}{\rho_f U_0^2 \pi r_s^2} = \frac{24}{\frac{\rho_f U_0 2r_s}{\mu_f}} = \frac{24}{Re}, \tag{4.14}$$

it is easy to realize that the drag coefficient should converge towards $C_D = 240$ since the Reynolds number was chosen to $Re = 0.1$. Regarding the displacement of the sphere, once steady state is reached both the acceleration and velocity goes to zero, $\ddot{x}_s = \dot{x}_s = 0$, and the governing equation may be written as

$$x_s = \frac{6\pi r_s \mu_f U}{k} = 0.1\pi \tag{4.15}$$

which also is confirmed by the solution.

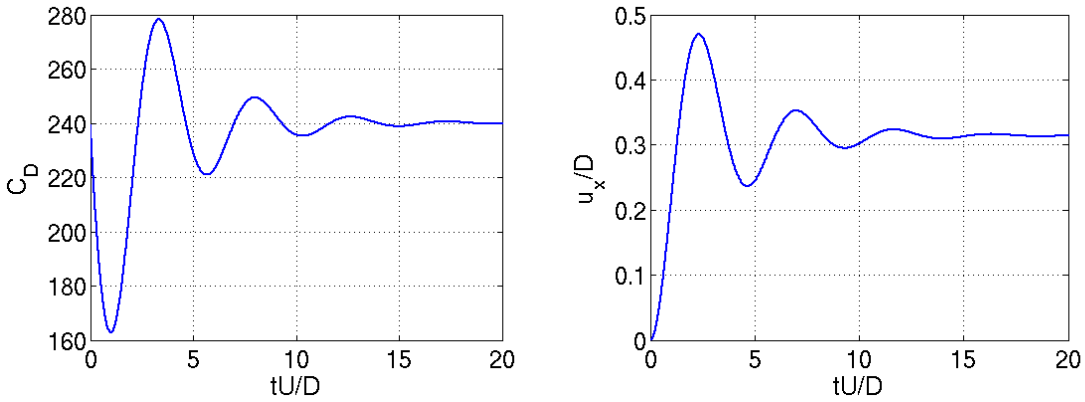

Figure 4.1: *Analytic solution of drag coefficient and displacement for an elastically mounted sphere.*

4.1.2 One Dimensional Solver

The one dimensional solvers is based on solving equation 4.1. The fluid solver is represented by the calculation of the drag force, as in equation 4.3 while the structural solver is represented by the calculation of

$$\ddot{x}_s = \frac{F_{Drag} - F_{Spring}}{m_s}. \tag{4.16}$$

The time step is set to $\Delta t = 40$ ms since it is the same as what was used during the three dimensional calculations described in next section. Firstly the problem is solved using the coupling method presented in algorithm 1. The result is shown in figure 4.2

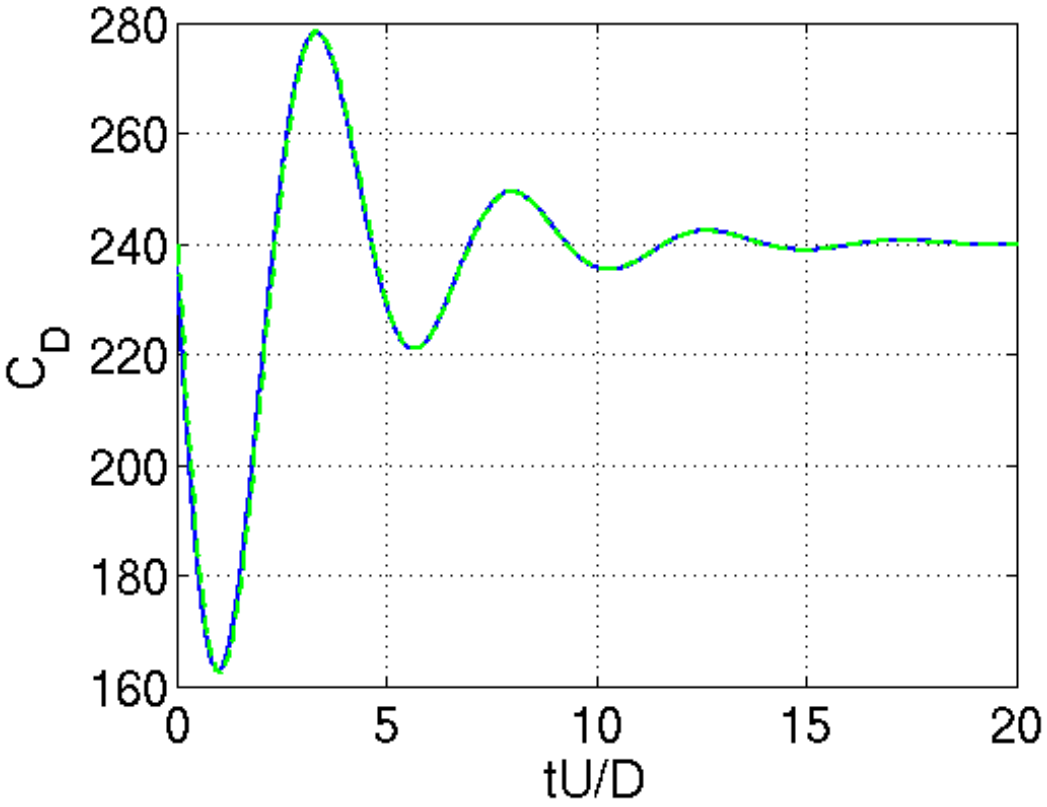

Figure 4.2: *Drag coefficient of an elastically mounted sphere. Comparison between the analytic solution (—) and the explicit coupling method (- - -) used in a one dimensional solver.*

As can be seen in the figure the simulated and analytic solution are virtually identical. The same goes for all of the interface predictor methods, as can be seen in figure 4.3. Meaning that conceptually none of them would give an inaccurate result. It can also be seen that the higher order predictors, —and —, give a more accurate result, which is also expected since the prediction of the position at the following time step should be more accurate.

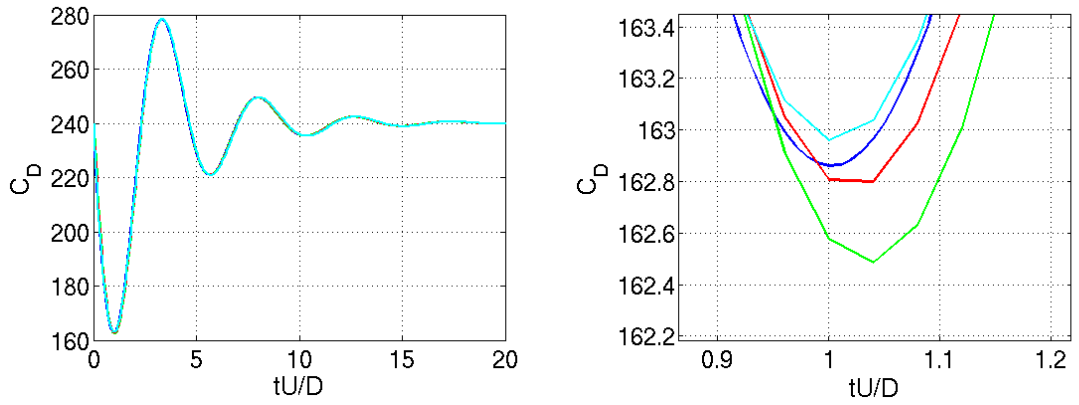

Figure 4.3: *Drag coefficient to the left and zoomed part to the right of an elastically mounted sphere. Comparison between the analytic solution (—) and the interface predicting coupling method with interface predicted according to equation 3.10 (—), equation 3.11 (—) and equation 3.12 (—) used with a one dimensional solver.*

Regarding the force predictor method presented in algorithm 3 it is expected that the results should to decrease in accuracy with decreasing β. A decreasing β undermines the ability to capture correct amplitudes during an oscillation, since the filtering of the forces causes the solution to "remember" previous forces. The result is presented in figure 4.4 and confirms the hypothesis. When β is set to 0.1 an accurate solution is still obtained but as β decreases to 0.01 the accuracy is sacrificed.

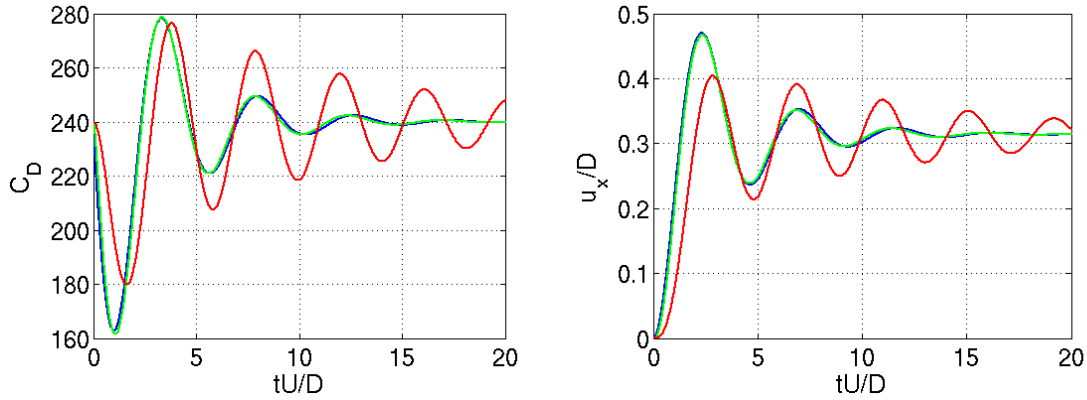

Figure 4.4: *Drag coefficient to the right and displacement to the left of an elastically mounted sphere. Comparison between the analytic solution (—) and the force predicting coupling method with $\beta = 0.1$ (—) and $\beta = 0.01$ (—) used with a one dimensional solver.*

The force smoothing method presented in algorithm 4 lacks in motivation why it should increase accuracy compared to the simpler explicit method presented in algorithm 1. Instead the motivation for this coupling is that it should increase the stability of the numerical simulation by making the transferred information between the two solvers more smooth over time. One should expect approximately the same behaviour from this coupling procedure as for the force predictor method. The re-

sult are presented in figure 4.5 and a similar behaviour as for the force predictor method is observed.

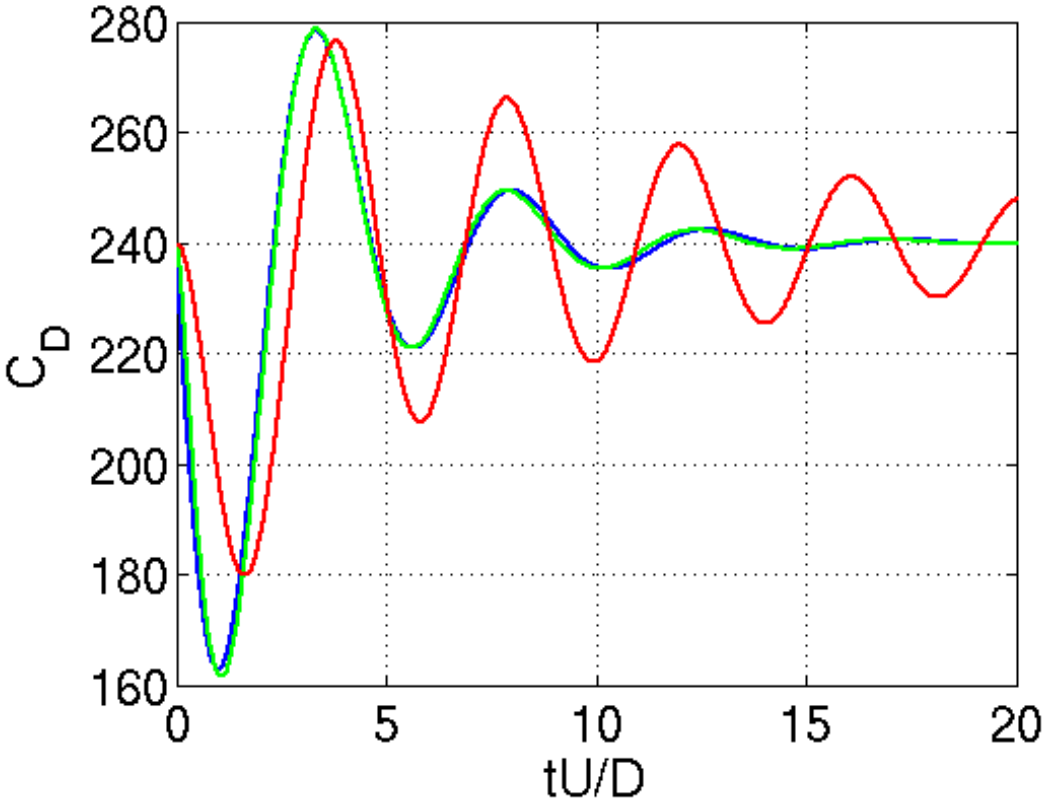

Figure 4.5: *Drag coefficient of an elastically mounted sphere. Comparison between the analytic solution (—) and the force smoothing coupling method with* $\beta = 0.1$ *(—) and* $\beta = 0.01$ *(—) used with a one dimensional solver.*

4.1.3 Numerical Results with IBOFlow and LaStFEM

In order to verify that the coupling methods has been properly implemented, the problem is also solved using the multiphase flow solver IBOFlow and the structural solver LaStFEM. Since Stokes flow has been assumed it is of importance that the numerical flow domain is chosen to be big enough so that the flow near the sphere is not affected from the external boundaries. Otherwise, the solution is not expected to agree with the analytic solution. In this thesis a domain size of $(100D \times 100D \times 100D)$, where D is the sphere diameter, was found to be big enough. The aim of this case has mainly been to validate that the implementation of the different coupling methods are correctly implemented and to study some tendencies in the solution obtained with the different coupling methods. Hence, no time step dependency or grid dependency study has been included in the thesis. Since this case consists of a three dimensional computational domain, the computational cost of conducting these dependency studies would have been quite high. The size of the cells near the boundaries of the sphere were set to $0.04D$ and the time step were chosen to be 0.04s, which corresponds to a Courant–Friedrichs–Lewy number of $CFL \approx 1$. A

slice of the computational domain with the grid for the fluid flow shown can be seen in figure 4.6.

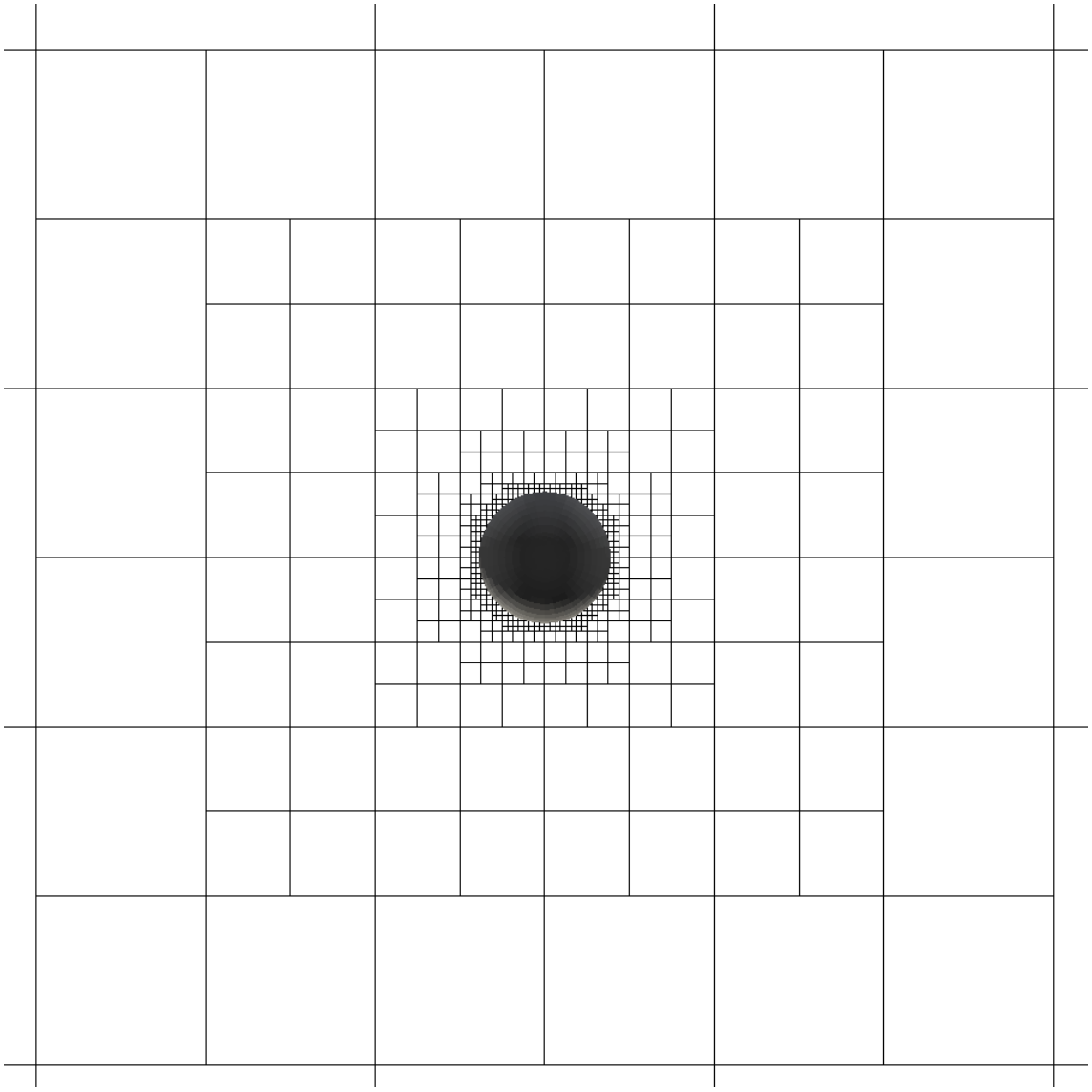

Figure 4.6: *Computational grid for the fluid flow around a elastically mounted sphere.*

Firstly the problem were solved using a the strong coupling method presented in algorithm 5. The result is shown in figure 4.7. The convergence criteria was set to $\varepsilon = 10^{-4}$ and an average of 4 iterations were needed in order to reach convergence, meaning that the computational cost is around 4 times greater compared to any weak coupling method. The numerical prediction has a good agreement with the analytic solution. Some white noise occurs in the drag force which indicates that averaging of the forces over time steps might be a good idea. The strong coupling method is the only coupling method included in this thesis that enforces equilibrium in each time step and is therefore the one that is expected to yield the most accurate result.

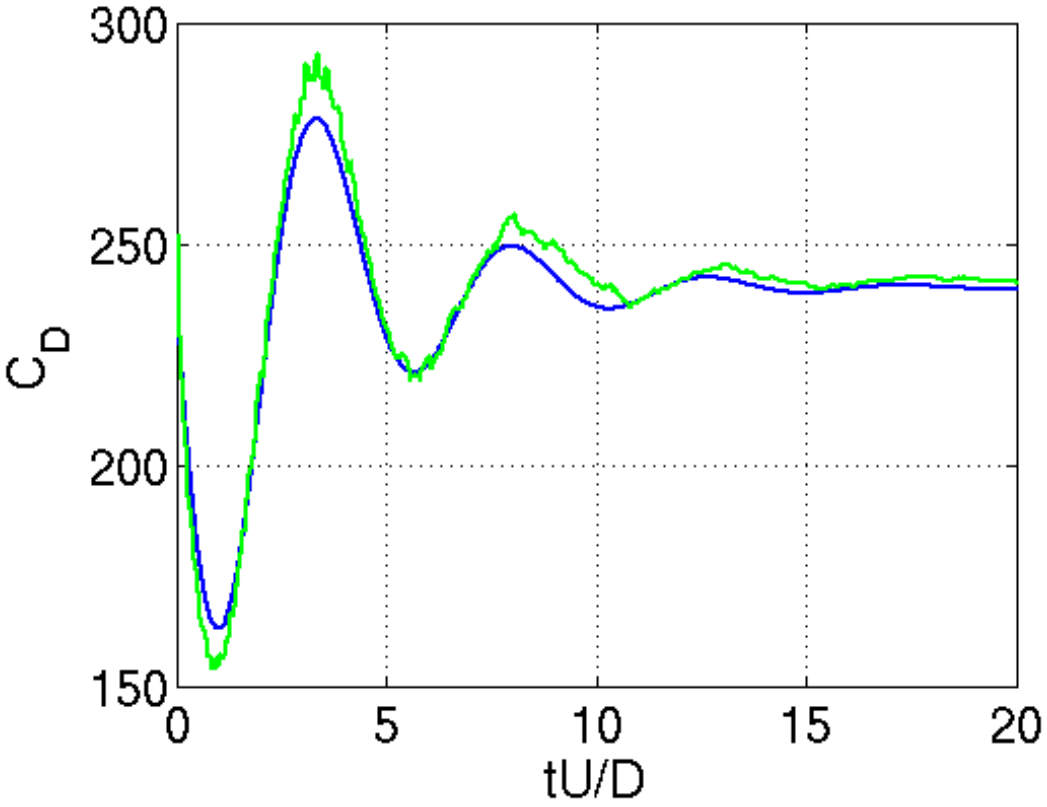

Figure 4.7: *Drag coefficient of an elastically mounted sphere. Comparison between the analytic solution (—) and the strong coupling method (—) used with the three dimensional solvers.*

Secondly the explicit coupling method presented in algorithm 1 was compared to the solution using the strong coupling algorithm 5. The result can be seen in figure 4.8 and the agreement between the two approaches is quite good. Some of the accuracy has been sacrificed in order to lower the computational cost, which was decreased with a factor of approximately 4. One can also observe that the amplitude of the white noise on the force has not decreased or increased, but remains approximately the same.

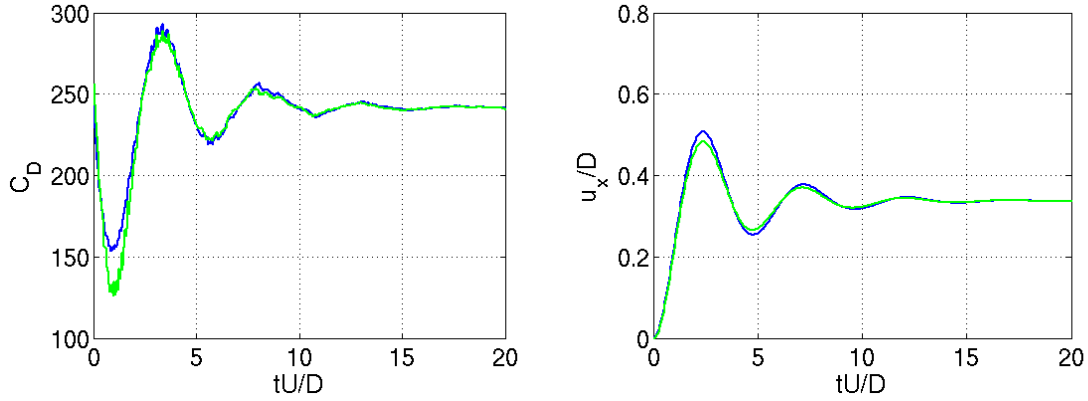

Figure 4.8: *Drag coefficient to the left and displacement to the right of an elastically mounted sphere. Comparison between the strong coupling method (—) and the explicit coupling method (—) used with the three dimensional solvers.*

In figure 4.9 the results are shown for the interface predicting method presented in algorithm 2 and compared to the one computed with the strong coupling. Excellent agreement for all of the coupling procedures can be be observed. Hence, it is concluded that for this specific problem it is much more efficient to use an interface predictor method compared to a strong coupling procedure, since barely no accuracy are sacrificed and the computational cost needed decreases with a factor of approximately 4.

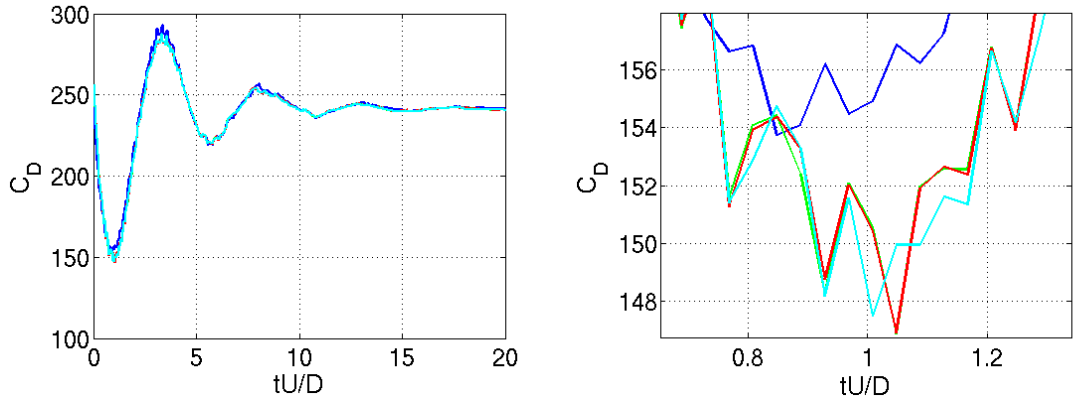

Figure 4.9: *Drag coefficient to the right and zoom to the left of an elastically mounted sphere. Comparison between the strong coupling method (—) and the interface predicting coupling method with interface predicted according to equation 3.10 (—), equation 3.11 (—) and equation 3.12 (—) used with the three dimensional solvers.*

Recall the result shown in figure 4.4 where the force predicting method presented in algorithm 3 was investigated using the one dimensional solvers. Since the time step used for both the one dimensional solver and the three dimensional solvers are the same, a similar behaviour regarding which β may be used before the accuracy are sacrificed should be expected. It was previously concluded that $\beta = 0.1$ gave a good

agreement while $\beta = 0.01$ undermined the solution. In figure 4.10 the hypothesis is confirmed. The solution is undermined when β decreases to $\beta = 0.01$. The oscillations becomes even bigger for $\beta = 0.01$ when using the three dimensional solver instead of the one dimensional solver. It can be explained by the small white noise that occurs on the forces in the three dimensional simulations. The force predicting method extrapolates forces from previous time steps in order to predict the acting force. If disturbances occur the extrapolation will increase these.

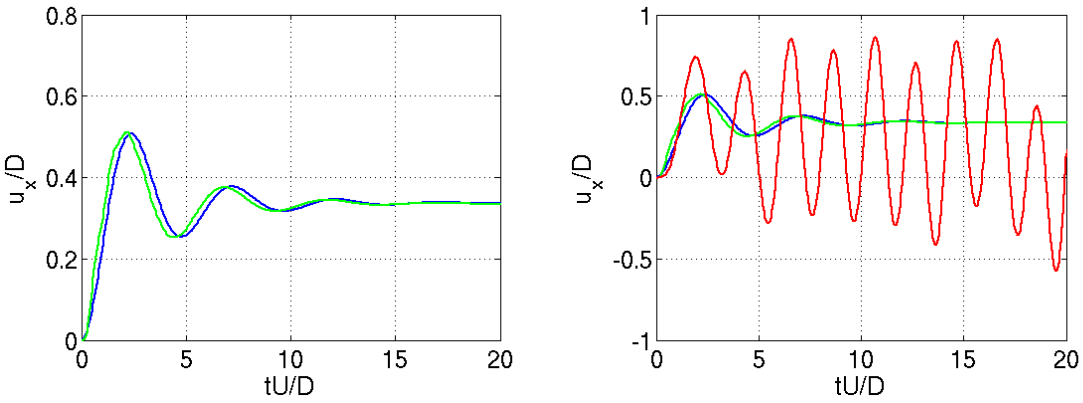

Figure 4.10: *Displacement of an elastically mounted sphere. Comparison between the strong coupling method (—) and the force predicting coupling method with $\beta = 0.1$ (—) and $\beta = 0.01$ (—) used with the three dimensional solvers.*

In the force smoothing method presented in algorithm 4 the forces are not extrapolated but only averaged over several time steps. Hence the force smoothing procedure is not expected to increase the oscillations as much as the force predictor methods at $\beta = 0.01$. The results are shown in figure 4.11. Regarding $\beta = 0.1$ a similar behaviour as for the force predicting method is observed. But as β decreases to 0.01 the oscillations has still increased compared to the one dimensional solution shown in figure 4.5 but not as severe as for the force predicting method.

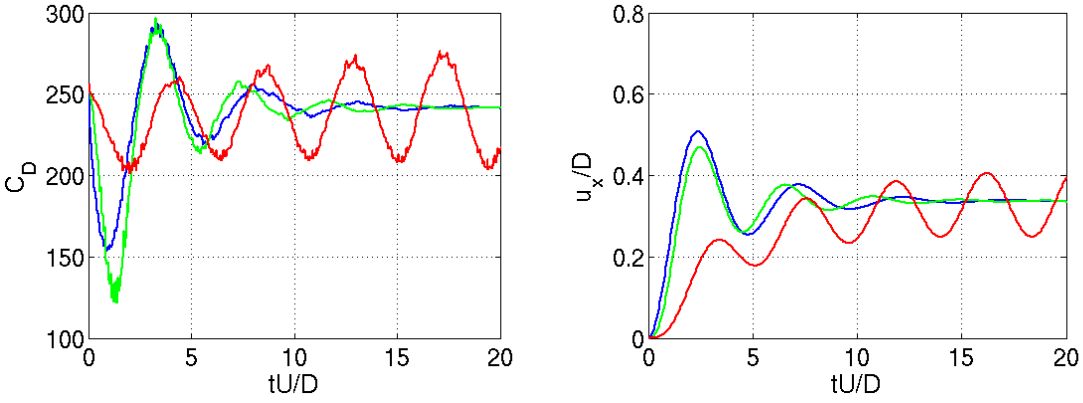

Figure 4.11: *Drag coefficient to the left and displacement to the right of an elastically mounted sphere. Comparison between the strong coupling method (—) and the force smoothing coupling method with $\beta = 0.1$ (—) and $\beta = 0.01$ (—) used with the three dimensional solvers.*

It can be observed that the amplitude of the oscillation of both the forces and the displacement increases over the complete simulation time when using the force smoothing method with $\beta = 0.01$. Intuitive, this is not an expected result since the only manipulation of forces is that they are filtered over time. But lets discuss this phenomenon. When using the force smoothing method a miss match between the fluid forces and the position and velocity of the sphere is created. When the filtering variable is set to $\beta = 0.01$, the acting force consists of 1% from the actual fluid force at the current time step and 99% from fluid forces at previous time steps. Stokes flow is assumed. Meaning that if the displacement of the sphere is decreasing (when the sphere is traveling in a opposite direction of the mean flow) the drag coefficient should be $C_D > 240$ and if the displacement is increasing $C_D < 240$. Since the force is filtered over time this is not true at all times for the sphere. Meaning that, even though the sphere is traveling down stream the force coefficient seen by the sphere can be $C_D > 240$. When this occurs, the turning point of the sphere occurs further down stream than what is actually physical. The opposite occurs when the sphere is traveling up stream. This causes the oscillations to increases over time. It should be noted that no extensive investigation has been done of this phenomenon, but the reasoning above has been made to provide some clarity for the interested reader.

4.1.4 Summary

In this section the proposed and implemented coupling methods has been validated and analyzed against a case where an analytic solution can be derived. All of the coupling methods showed good agreement with the analytic solution, which suggest that the implementation is correct and that the coupling methods have good potential. All of the weak coupling methods where approximately four times more efficient than the strong coupling method. The interface predicting methods slightly increased the accuracy compared to the explicit coupling method. Neither one of the force predicting or force smoothing methods increased the accuracy compared to the explicit coupling procedure. But since the aim of these methods is not to increase accuracy but increase stability, this was not expected. If β is decreased too much the accuracy of the solution is undermined.

4.2 Numerical Case: Rigid Cylinder Attached to a Damped Spring in an Incompressible Laminar Flow

In order to study the accuracy and the stability of the different coupling algorithms a rigid cylinder attached to a damped spring in a moderate Reynolds number flow is studied. The case has previously been studied in [33], [55] and [56].

The equation of motion for the cylinder may be written in non-dimensional quantities as

$$\ddot{\boldsymbol{\xi}}_s + 2\zeta \left(\frac{2\pi}{U^*}\right) \dot{\boldsymbol{\xi}}_s + \left(\frac{2\pi}{U^*}\right)^2 \boldsymbol{\xi}_s = \frac{2}{\pi\rho}\mathbf{C} \tag{4.17}$$

where $\boldsymbol{\xi}_s = \frac{1}{D}\mathbf{x}_s$ is the dimensionless displacement vector, D is the diameter of the cylinder, $\mathbf{x_s}$ are the displacement vector. $\dot{(\,)} = \frac{\partial(\,)}{\partial tU/D}$ is the dimensionless time derivative, t is the time and U is the free stream velocity. $\zeta = c/2\sqrt{km_s}$ is the damping ratio, c is the damping coefficient, k is the spring constant and m_s is the mass of the cylinder. $U^* = U/(f_N D)$ is the reduced velocity and $f_N = 1/(2\pi)\sqrt{k/m_s}$ is the natural frequency. $\rho = \rho_s/\rho_f$ is the solid-to-fluid density ratio, ρ_s is the solid density and ρ_f is the fluid density. $\mathbf{C} = 2\mathbf{F}/(\rho_f U^2 D)$ is the fluid force coefficient and $\mathbf{F}$ is the fluid force. The dimensionless material parameters are $\zeta = 0.01,\ U^* = 5, \rho = 4/\pi$ and the Reynolds number is 200.

In order to set up an actual simulation, which would correspond to an physical problem, some parameters needs to be chosen. The parameters that needs to be determined are the free stream velocity, U, fluid density, ρ_f, dynamic viscosity, μ_f, cylinder diameter, D, solid density, ρ_s, damping coefficient, c, and spring constant, k. Meaning that there are four constraints and seven parameters. Lets choose

$$U = 1 \text{ m/s}, \quad D = 1 \text{ m} \quad \text{and} \quad \rho_f = 1 \text{ kg/m}^3 \tag{4.18}$$

and the rest of the parameters can be calculated as

$$\begin{aligned} \mu_f &= \frac{\rho_f U D}{Re} \\ \rho_s &= \rho_f \rho \\ k &= \rho_s \pi \left(\frac{D}{2}\right)^2 \left(2\pi \frac{U}{U^* D}\right)^2 \\ c &= 2\zeta \sqrt{k \rho_s \pi \left(\frac{D}{2}\right)^2}. \end{aligned} \tag{4.19}$$

The parameters are summarized in table 4.2.

Table 4.2: *Used parameters for an elastically mounted cylinder with $\rho = 4/\pi$.*

U [m/s]	ρ_f [kg/m^3]	μ_f [kg/ms]	D [m]	ρ_s [kg/m^3]	k [N/m]	c [Ns/m]
1	1	1/200	1	$4/\pi$	$4\pi^2/25$	$\pi/125$

The computational domain, the cylinders initial position and the boundary condition is shown in figure 4.12. The cylinder is initially placed in $(x, y) = (0, 0)$, the lower corner of the computational domain is placed in $(x, y) = (-10D, -10D)$ and the upper corner is placed in $(x, y) = (30D, 10D)$. At the inlet, $x = -10D$, a uniform velocity profile is applied and at the outlet, $x = 30D$, a zero pressure boundary condition is applied. At $y = -10D$ and $y = 10D$ no slip boundary conditions are applied with the same velocity as at the inlet. At the interface of the cylinder a no slip boundary condition is applied.

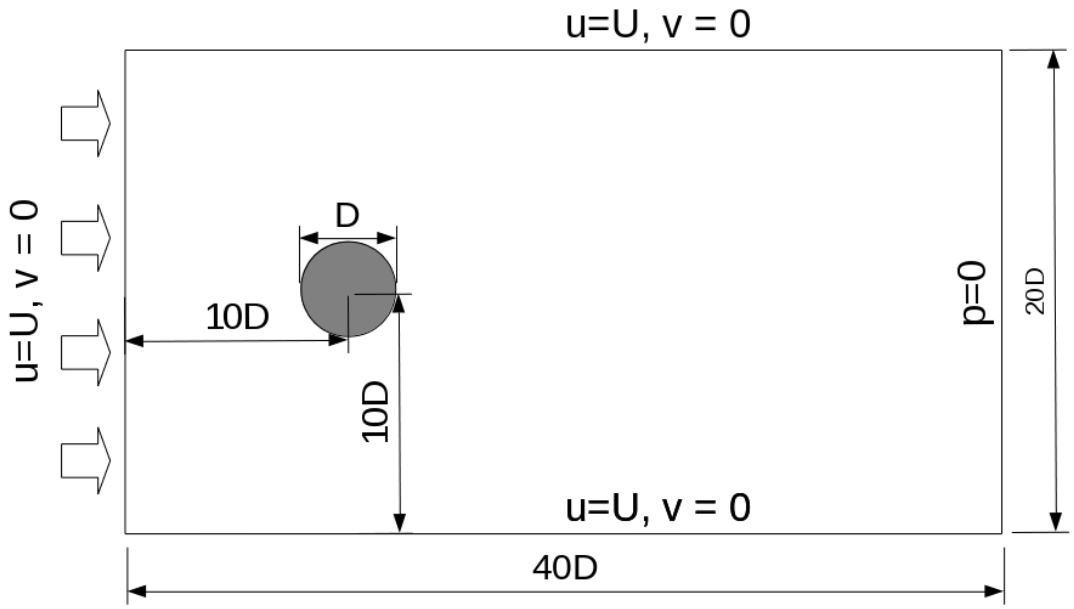

Figure 4.12: *A schematic diagram of the computational domain for an elastically mounted cyliner with the boundary condition and initial placement of the cylinder. Note that the diagram is not to scale.*

The computational domain is discretized in space using quadratic cells and a constant time step in time. The spatial discretization is rebuild at each time step so that the smallest cells are placed at the interface between the solid and the fluid. The baseline grid can be seen in figure 4.13 which consists of approximately 36000 cells and the smallest cell size is $\Delta x = \Delta y = 0.005D$.

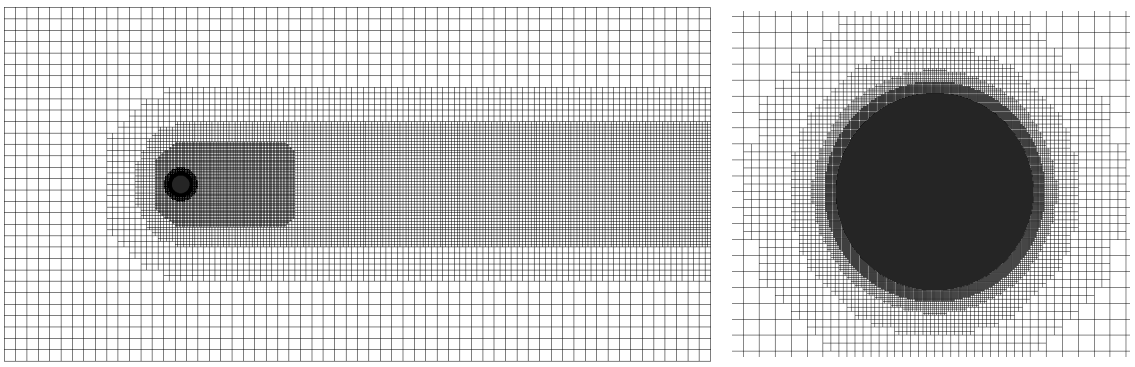

Figure 4.13: *Computational grid for an elastically mounted cylinder with* $\Delta x_{min} = \Delta y_{min} = 0.005D$ *and approximately 36000 cells. Complete domain to the left and zoom near the cylinder to the right.*

In order to avoid instabilities and large fluid forces that might occur during the first time steps, when the flow field undergo large changes and might be nonphysical, the corresponding stationary cylinder problem was first solved using only the fluid solver. When a fully developed, periodic, flow field was obtained, the FSI problem was solved. In order to reduce the computational time needed for each problem the

stationary cylinder problem was solved on a coarser grid and interpolated onto the grid used for the specific case. This also allowed each FSI simulation to be started from the exactly the same flow field, meaning that the dynamic behaviour before the periodic state was reached could also be included in the analysis of different couplings and spatial and temporal dependencies. The end time for the simulations was determined by when a periodic steady state behaviour was reached and had occurred for at least a couple of periods.

4.2.1 Validation for Strong Coupling Method

The aim of the analysis is to compare accuracy and stability of different weak coupling methods. The result will both be compared between different coupling methods and to previous work. Hence, it is of interest to reassure that temporal and spatial convergence is reached, meaning that the solution has a "small enough" dependency on the grid and on the time step. This is done by conducting a time step dependency study and a mesh dependency study using the most stable coupling method, the strong coupling method. The variable which has been chosen for comparison between the different computations is the amplitude of the oscillations in $y-$direction. The different combinations of time step and smallest cell size that has been used are presented in table 4.3

Table 4.3: *Simulated combination, marked by x, of spatial discretization and temporal discretization for a elastically mounted cylinder with $\rho = 4/\pi$.*

		Δt [ms]				
		64	32	16	8	4
Δx_{min} [mm]	40					x
	20					x
	10					x
	5	x	x	x	x	x
	2.5					x

In order to assure that equilibrium is reached at each time step a convergence criteria of $\varepsilon = 10^{-4}$ was set. An average of 4 iterations were needed at each time step to fulfill this criteria. The temporal and spatial convergence can be seen in figure 4.14. Both the temporal and spatial convergency ratio approaches second order as the time step and the cell size decreases, which indicates that the results only has a small dependecy on the discretization used at these sizes. Hence, a time step of $\Delta t = 4$ ms and a smallest cell size of $\Delta x_{min} = 5$ mm is chosen to be used during the accuracy and stability analysis with the weak coupling algorithms.

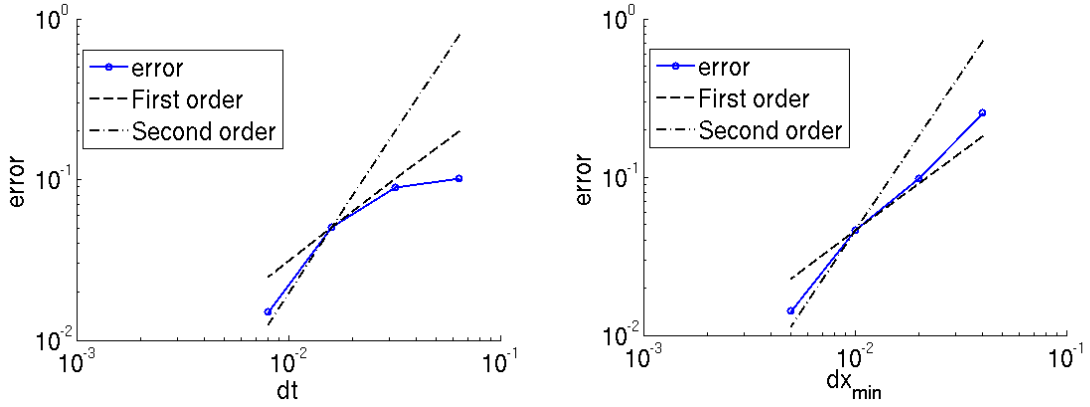

Figure 4.14: *Temporal convegence to the left and spatial convergence to the right of a elastically mounted cylinder with $\rho = 4/\pi$. The error were determined as error $= (u_y(\Delta t_{ref}, \Delta x_{min,ref}) - u_y(\Delta t, \Delta x_{min}))/u_y(\Delta t_{ref}, \Delta x_{min,ref})$ where $\Delta x_{min,ref} = \Delta x_{min} = 5$ mm and $\Delta t_{ref} = 4$ ms for the temporal convergence and $\Delta t_{ref} = \Delta t = 4$ ms and $\Delta x_{min,ref} = 2.5$ mm for the spatial convergence.*

In figure 4.15 the results obtained are compared to the results from previous studies. After some time the cylinder's trajectory reaches a periodic state where the trajectory draws a figure of eight, which is shown in the figure. The trajectory of this periodic state agree well with both [55] and [33] but the trajectory of [56] is shifted slightly downstream due to a 3% difference in drag force.

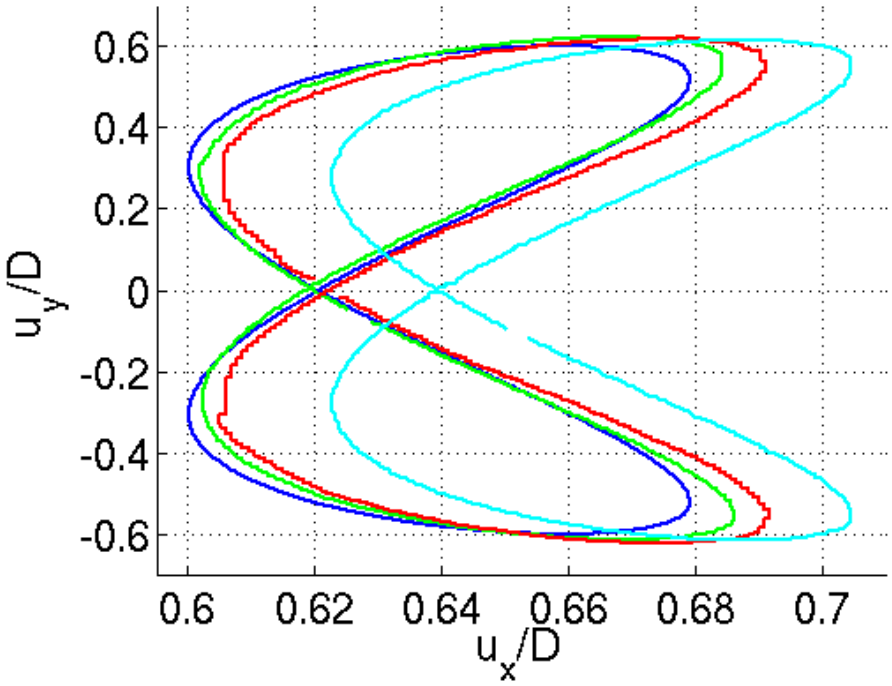

Figure 4.15: *Trajectories of the center of an elastically mounted cylinder with $\rho = 4/\pi$ when the periodic state is reached. Result computed with the strong coupling method (—) and results from previous studies (—) [55], (—) [33] and (—) [56].*

In figure 4.16 the trajectory of the cylinder during the complete simulation time is shown. As expected some transient oscillation occur before the periodic state is reached. The same phenomenon can also be observed by studying the displacement over time which is shown in the same figure.

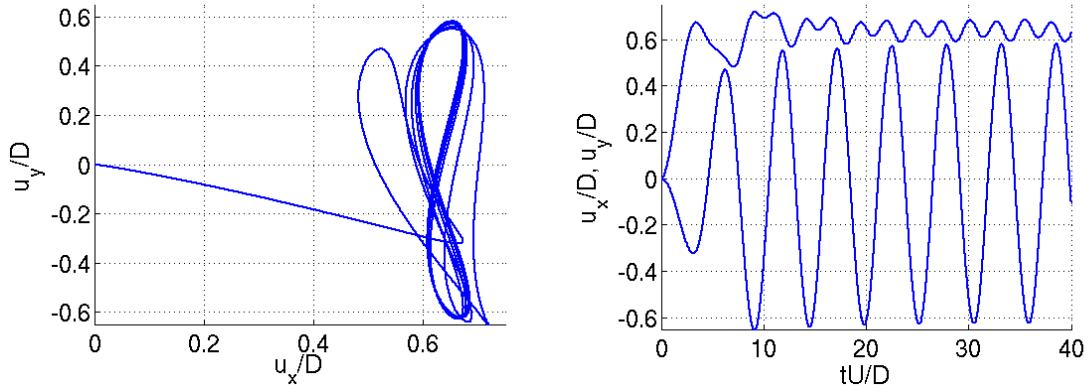

Figure 4.16: *Trajectory to the left and displacement in both x- and y-direction over time to the right of an elastically mounted cylinder with $\rho = 4/\pi$ computed with the strong coupling method.*

The drag coefficient and lift coefficient can be seen in figure 4.17. Here one may observe the white noise occurs in the force signal. Furthermore both the drag and lift coefficient behaves as expected.

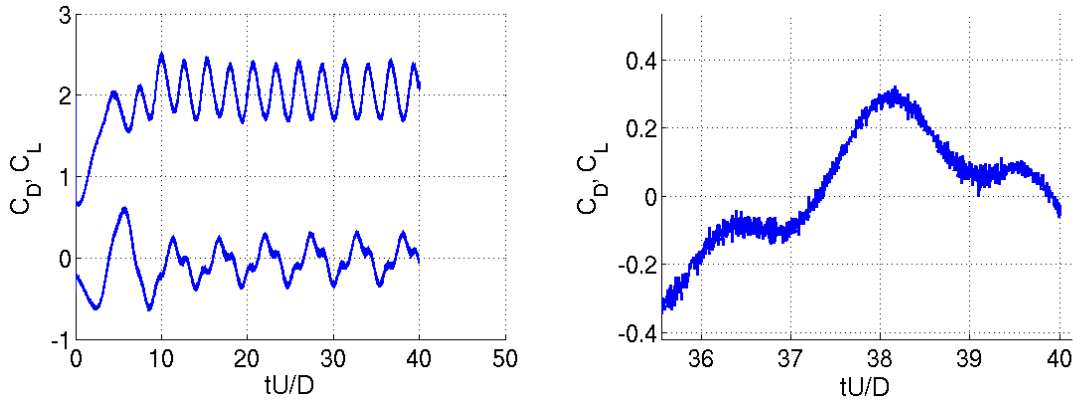

Figure 4.17: *Drag and lift coefficient acting on the cylinder over time to the left and a zoom to the right of an elastically mounted cylinder with $\rho = 4/\pi$ computed with the strong coupling method.*

In figure 4.18 the contours of the vorticity in the flow field is shown. One can observe the characteristic vortex street which is created down stream of a cylinder, which is expected at moderate Reynolds numbers. At some vorticies a discountinuity may be observed, which can be explained by the fact that the grid size changes in size in those regions and some parts of the vortices can not be resolved by the grid anymore. The vortex shedding creates two single vortices in each period and agree well with the vortex shedding shown in both [33] and [56].

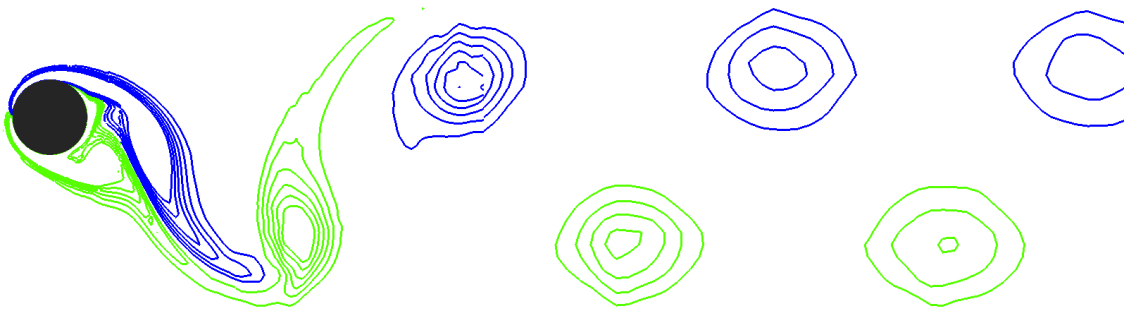

Figure 4.18: *Countours of the instantaneous vorticity of an elastically mounted cylinder with $\rho = 4/\pi$. (—) indicates negative vorticity while (—) indicates positive vorticity.*

In total one can state that the result obtained using the strong coupling agrees well with those of previous studies. Temporal and spatial convergence was reached and the convergency ratio has been deemed as second order both in space and time. The spatial discretization which was chosen to proceed with consists of approximately 36000 cells and the smallest cell has the size $\Delta x = \Delta y = 5$ mm. The time step were chosen to 4 ms and at this density ratio a simulation time of 40 s was needed in order to reach the periodic state. An average of 4 iterations was needed in order to reach the convergence criteria. In the following accuracy and stability analysis this coupling will be used as the baseline case and assumed to give the accurate result.

The stability of the coupling method will be investigated by decreasing the density of the structure. As has been discussed in the theory section, a decreasing solid-to-fluid density ratio is a well known cause of instabilities when dealing with fluid structure interaction problems. Hence, the stability analysis is conducted by decreasing the density ratio until instability is reached. The result at the lowest density ratio is also compared to the result obtained by using the strong coupling method to be able to determine the accuracy of the coupling at the brink of instability.

In practice the solid-to-fluid density ratio, ρ, is changed and the new parameters are calculated so that equation 4.18 and 4.19 are still fulfilled. A decreasing solid-to-fluid density ratio, ρ, causes a decreasing solid density, ρ_s, which causes a decreasing spring constant, k, and a decreasing damping coefficient, c. The drag coefficient will not experience any large changes since the Reynolds number remains constant, meaning that the displacement in x-direction, u_x, will increase as the solid-to-fluid density ratio decreases. At some density ratio the displacement will become so large that the cylinder will pass through the outlet and leave the domain. Meaning that there exist a limitation on how far this case can be used regarding stability analysis based on a decreasing solid-to-fluid density ratio. However, to the authors knowledge, this limit has not been reached when using weak coupling algorithms by any previous analysis. [56] reached a solid-to-fluid density ratio of $\rho = 1.08$ using a weak coupling algorithm before stability issues were encountered and [33] reached a solid-to-fluid density ratio of $\rho = 0.21$ using a weak coupling algorithm.

4.2.2 Explicit Coupling Method

The explicit coupling presented in algorithm 1 is the most simple method included in this thesis. The method do not consist of any predictions or manipulations of the forces exerted by the fluid on the structure interface. Hence, the accuracy and stability of this coupling will be investigated and discussed first. In figure 4.19 the trajectories and the displacement over time is compared to the ones calculated with the strong coupling method. The agreement between the explicit coupling method and the strong coupling method are excellent. The only difference that can be observed regarding the displacement are that the explicit coupling method seem to slow down the frequency of the oscillations, but just marginal.

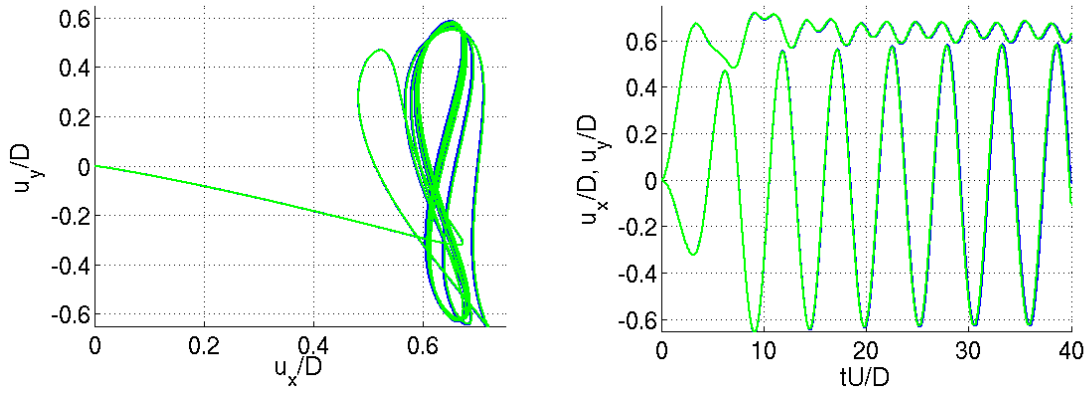

Figure 4.19: *Trajectories to the left and displacement against time to the right of an elastically mounted cylinder with $\rho = 4/\pi$. Comparison between the explicit coupling method (—) and the strong coupling method (—).*

In figure 4.20 the calculated force coefficients are shown and compared to the ones calculated using the strong coupling. A similar white noise as has been observed for the strong coupling still occurs but it can be observed that the white noise has increased in amplitude compared to the strong coupling, but only marginally. The behaviour of the forces are in excellent agreement for both coupling methods, hence the conclusion that the explicit coupling is suitable for this case at this density ratio is drawn.

Regarding the computational cost an average of 4 iterations were needed in order to achieve convergence for the strong coupling method, meaning that using the explicit coupling method yielded an accurate result using only one fourth of the computational cost.

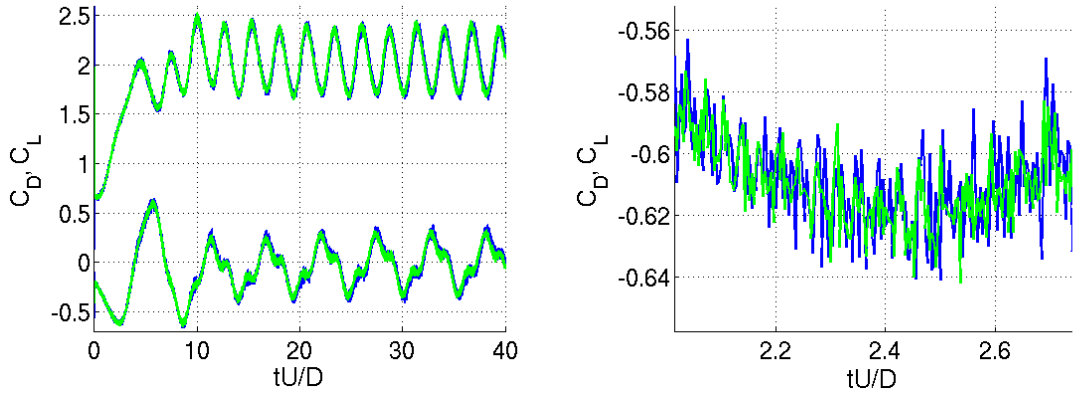

Figure 4.20: *Force coefficients plotted over time to the left and a zoomed part to the right of an elastically mounted cylinder with $\rho = 4/\pi$. Comparison between the explicit coupling method (—) and the strong coupling method (—).*

The method was found to be equally stable as the strong coupling method down to a solid-to-fluid density ratio of 0.46. In figure 4.21 the results from explicit coupling method is presented and compared to those computed using the strong coupling method. By studying the difference in the computed displacement it can be concluded that the agreement between the strong coupling method and the explicit method is excellent for all solid-to-fluid density ratios where the explicit coupling is still stable. But if one studies the force coefficients, the white noise has increased drastically when using the explicit coupling algorithm. It is even difficult to determine anything from the signal. But since the agreement between the displacements are excellent the mean signal of the force coefficients must follow the signal computed by using the strong coupling. However, the reason for instabilities at smaller density ratios is due to this white noise in the force signal. Regarding the computational cost an average of a little over four iterations were needed in order to reach convergence.

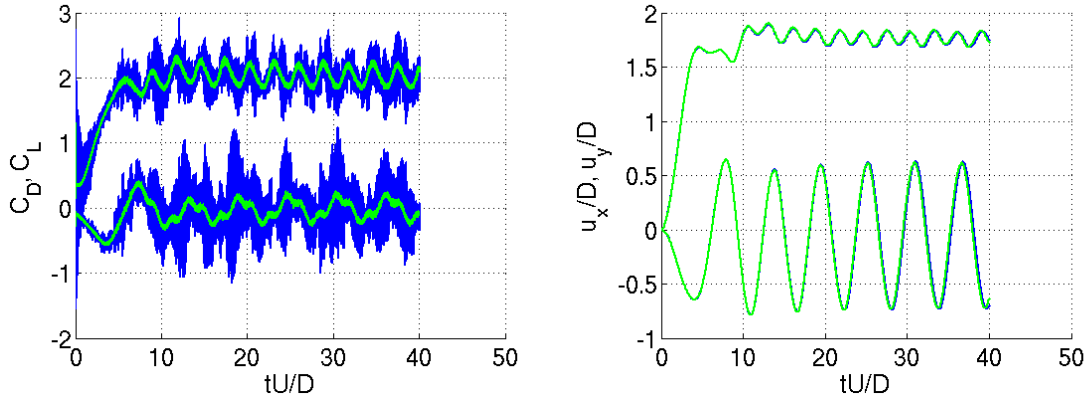

Figure 4.21: *Force coefficients plotted over time to the left and displacement in both x- and y-direction to the right of an elastically mounted cylinder with $\rho = 0.46$. Comparison between the explicit coupling method (—) and the strong coupling method (—).*

The explicit coupling method has been proven to yield accurate results at the density ratios where it is still stable. The explicit coupling method was approximately four times more efficient compared to the strong coupling method.

4.2.3 Interface Predicting Method

When using a weak coupling based on an interface predicting method the idea is to predict the position, velocity and acceleration of the interface at the current time step depending on the position, velocity and acceleration at the previous time step, or time steps. The hypothesis is that this will increase the accuracy and hence, the stability of the computations. In figure 4.22 the problem has been solved using the interface predicting method, presented in algorithm 2, with the interface predicted according to equation 3.10. The result is clearly affected by the coupling method, but not in the way that one would hope for. The accuracy has been seriously undermined. The explicit coupling method, analyzed in the previous section, gave an excellent agreement with the strong coupling algorithm while this method results in a considerable offset in both displacement and forces.

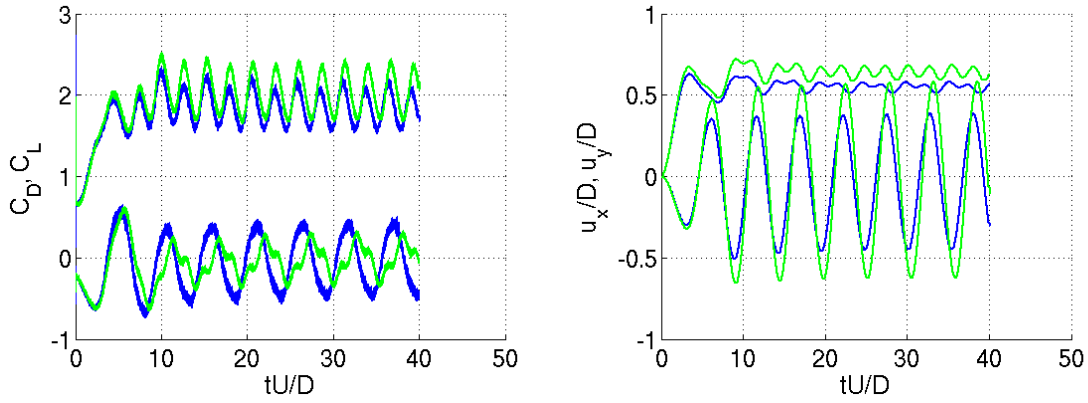

Figure 4.22: *Force coefficients plotted over time to the left and displacement in both x- and y-direction to the right of an elastically mounted cylinder with $\rho = 4/\pi$. Comparison between the interface predictor coupling method (—) with interface predicted as equation 3.10 and the strong coupling method (—).*

In figure 4.23 the result computed using the interface predicting method with the three different implemented predictions (equation 3.10, 3.11 and 3.12) are all presented. The results are virtually identical. Meaning that regardless of which prediction that are used an offset in both displacement and forces are created.

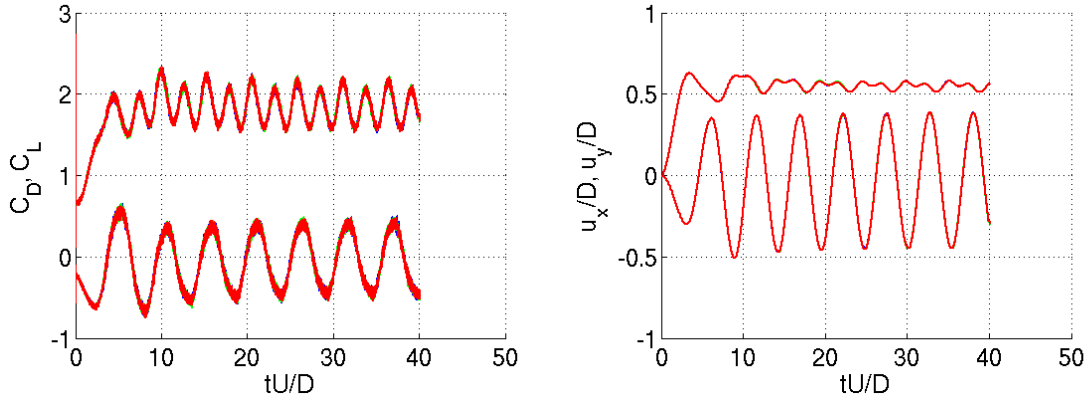

Figure 4.23: *Force coefficients plotted over time to the left and displacement in both x- and y-direction to the right of an elastically mounted cylinder with $\rho = 4/\pi$. Comparison between the interface predicting coupling method with interface predicted as equation 3.10 (—), 3.11 (—) and 3.12 (—).*

Lets discuss the three different coupling methods that has been used to solve this problem so far in the thesis. Firstly the problem was solved using the strong coupling presented in algorithm 5. The algorithm basically consists of "guessing" that the structure is at the same position as at the previous time step, solving fluid field, calculating the stresses acting on the structural interface, let the forces act on the interface and solving structural equations and iterate between the solvers until equilibrium is reached and the final position of the structure is obtained. The explicit coupling method may be summarized as "guessing" the position of the structural interface as the same as at the previous time step, solving fluid field, calculating fluid forces and let the forces act on the structure and solve structural equations in order to obtain the final position. When using the interface predicting method presented in algorithm 2 the position of the interface is firstly "guessed" according to equation 3.10, 3.11 or 3.12, the fluid field is solved, the fluid forces are calculated and applied to the structural interface in order to obtain the final position.

All three of these methods consists of a "guessed" position and a final position. Hence, it is of interest to investigate if the guessed position is more accurate when using an interface predicting coupling method compared to a explicit coupling method. Since all three of the interface predictor methods yielded virtually identical results, only the prediction according to equation 3.10 will be investigated.

The result computed by using the strong coupling method is assumed to be the correct one and the "guessed" position, $\tilde{\mathbf{x}}^n$, at the current time step is computed using both the explicit coupling method and interface predictor method. The deviation,ε^n, from the equilibrium state,$\mathbf{x}^n$ (the one computed through iterations by the strong coupling), is then calculated as

$$\varepsilon^n = ||\mathbf{x}^n - \tilde{\mathbf{x}}^n||. \tag{4.20}$$

The deviation,ε^n, of the explicit coupling method and the interface predicting method with the interface predicted according to equation 3.10 is shown in figure 4.24.

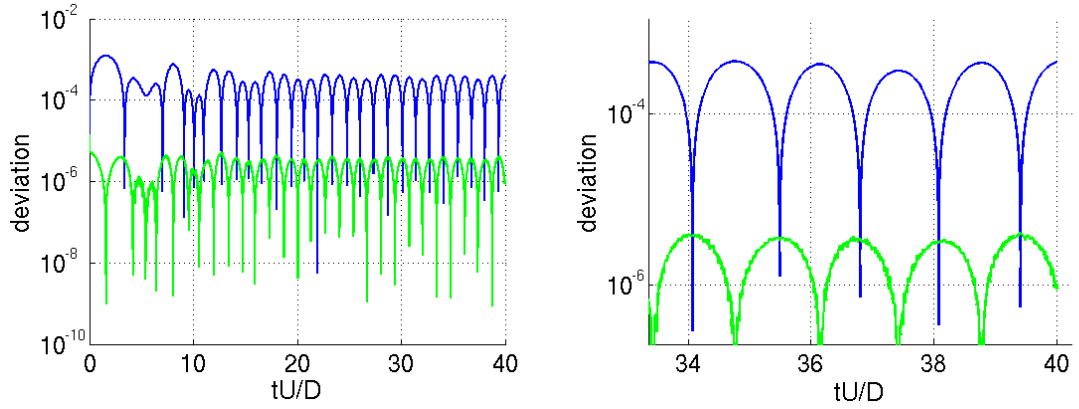

Figure 4.24: *Deviation, ε^n, in "guessed" position, $\tilde{\mathbf{x}}^n$, from correct one, $\mathbf{x}^n$, to the left and zoom to the right of an elastically mounted cylinder with $\rho = 0.46$. Comparison between the explicit coupling method (—) and interface predicting coupling method with interface predicted as equation 3.10 (—).*

The deviation of the interface predicting method is much smaller than the one for the explicit coupling method. Hence, the interface predictor method should yield a more accurate result. One could also note that it can be seen in the figure that the place where the deviation is the smallest for the explicit method, the deviation reaches its larges values for the interface predicting method. This can be explained by the fact that when using the explicit coupling method the guessed value would be identical with the correct one if the velocity is zero, which occurs at the maximum displacement in y-direction while the guessed position for the interface predicting method would be the correct one if the velocity is constant, which occurs at the minimum displacement in y-direction.

The problem persists, the cause of the error in accuracy when using the interface predictor methods remains unknown. The author has investigated the code and the result in order to reach a conclusion, but has not succeeded in providing an answer. The implementation has been validated in section 4.1, where the expected increase, compared to the explicit coupling method, in accuracy were achieved.

However, even though the method seems to undermine the accuracy it is still of interest to investigate how the interface predicting method affects the stability of the simulations. All three of the implemented prediction models (equation 3.10, 3.11 and 3.12) were stable down to solid-to-fluid density ratio of $\rho = 0.46$, which is the same as for the explicit coupling method. The results are still virtually identical for all prediction models. Hence, only the results computed with the interface predicted according to equation 3.10 is shown and compared to the results computed with the strong coupling method in figure 4.25. A similar offset in displacement as for the solution with $\rho = 4/\pi$ can be observed. Regarding the force coefficient the white noise has increased as the solid-to-fluid density ratio decreased, as it did for the explicit coupling algorithm. If one would compare the results in figure 4.25 computed with the interface predicting method at $\rho = 0.46$ with the one computed with the explicit coupling at the same density ratio in figure 4.21 it may be observed that the

white noise in the force signal has increased less when using a interface predicting method. If the displacement computed with the two methods would have been the same, this would be an indication of increased stability. But since this is not the case, no conclusions can be drawn from this observation.

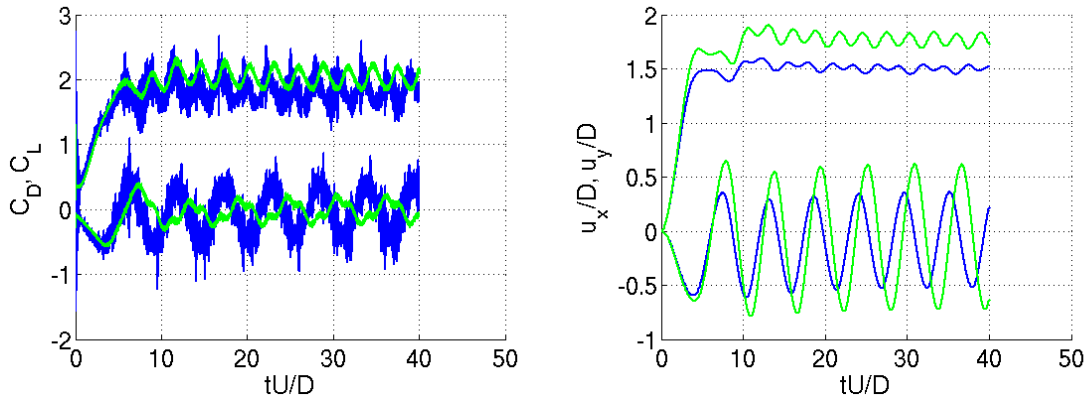

Figure 4.25: *Force coefficients plotted over time to the left and displacement in both x- and y-direction to the right of an elastically mounted cylinder with $\rho = 0.46$. Comparison between the interface predictor coupling method (—) with interface predicted as equation 3.10 and the strong coupling method (—).*

The interface predicting method yielded a virtually identical result regardless of how the interface was predicted. The agreement in result between the method and the strong coupling method was much lower compared to the explicit coupling method. The method were stable down to a solid-to-fluid density ratio of $\rho = 0.46$, which is the same as for the explicit coupling method.

4.2.4 Force Predicting Method

Setting $\beta = 1$ when using the force predicting method presented in algorithm 3 means that no filtering over time of the forces is performed, only an extrapolation of forces in time. Due to the white noise in the force signal this could prove problematic. The force predicting method has been used together with $\beta = 1$, $\beta = 0.33$ and $\beta = 0.1$. At the solid-to-fluid density ratio $\rho = 4/\pi$ both $\beta = 1$ and $\beta = 0.33$ became unstable and ρ needed to be increased in order to achieve stable solutions. However, for $\beta = 0.1$ a stable solution could be produced for $\rho = 4/\pi$. The results are shown in figure 4.26. The results experience a considerable offset in both fluid forces and displacement.

Since this method yielded instabilities at much higher density ratios compared to other methods and poor solutions when stable solutions could be produced only a small amount of time was dedicated to investigating the method. With $\beta = 1$ the stability limit was reached at density ratio of $\rho = 1.5$, with $\beta = 0.33$ the stability limit was reached at density ratio of $\rho = 1.4$ and with $\beta = 0.1$ the stability limit was reached at density ratio of $\rho = 1.1$.

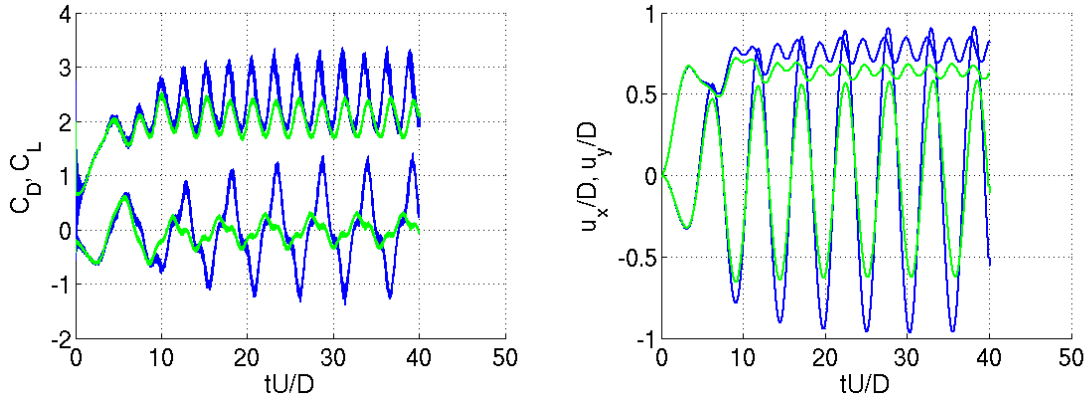

Figure 4.26: *Force coefficients plotted over time to the left and displacement in both x- and y-direction to the right of an elastically mounted cylinder with $\rho = 4/\pi$. Comparison between the force predictor coupling method (—) with $\beta = 0.1$ and the strong coupling method (—). Note that the showed force coefficients are as computed by the fluid solver and not the force coefficients seen by the structure.*

Lets study what happens if we take the data produced by using the strong coupling and predict the fluid forces at the next time step depending on the previous ones, as proposed in algorithm 3. The result is shown in figure 4.27 where it can be seen that using this predictor model increases the amplitude of the white noise in force signal. This is the reason why this method has more stability problems compared to other models.

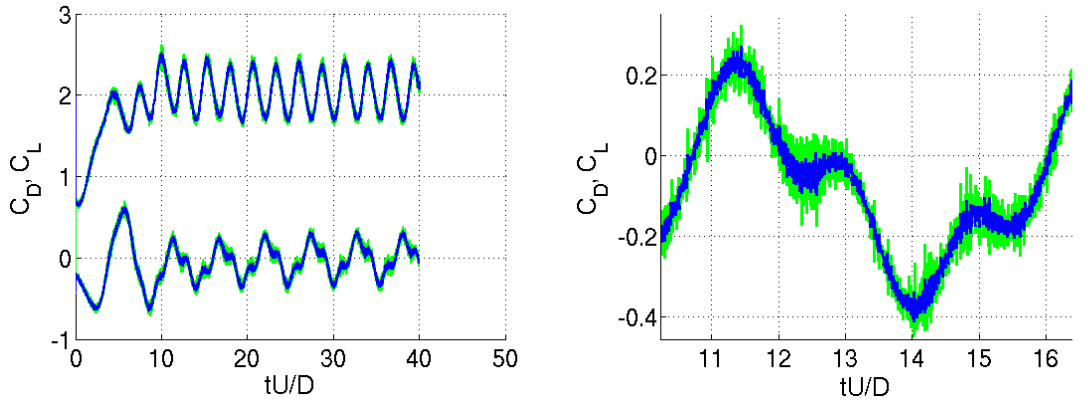

Figure 4.27: *Force coefficients plotted over time to the left and zoom to the right of an elastically mounted cylinder with $\rho = 4/\pi$. Strong coupling method with actual force coefficient (—) and force coefficient predicted according to the force predicting method (—) with $\beta = 1$.*

4.2.5 Force Smoothing Method

The force smoothing method presented in algorithm 4 becomes identical with the explicit coupling method if β is set to one. Hence the analysis will only cover smaller values. The analyzed values has been $\beta = 0.33$, $\beta = 0.1$, $\beta = 0.033$ and

$\beta = 0.01$. The results for $\beta = 0.33$ is presented in figure 4.28 and compared to the ones obtained with the strong coupling method ($\rho = 4/\pi$). The agreement is excellent. Hence, it can be concluded that with $\beta = 0.33$ the filtering of forces does not undermine the result.

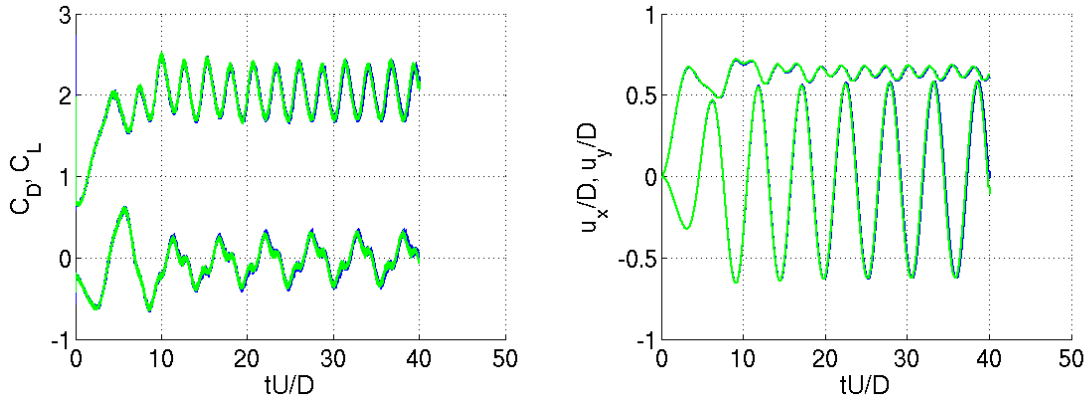

Figure 4.28: *Force coefficients plotted over time to the left and displacement in both x- and y-direction to the right of an elastically mounted cylinder with $\rho = 4/\pi$. Comparison between the force smoothing method (—) with $\beta = 0.33$ and the strong coupling method (—). Note that the showed force coefficients are as computed by the fluid solver and not the force coefficients seen by the structure .*

It is obvious that if β is chosen too small the solution will be inaccurate. In order to investigate how the solution depends on β the solution at the solid-to-fluid density ratio $\rho = 4/\pi$ has been compared with the different choices of β. The error in both oscillation amplitude, $u_{y,max}$ and x-position of where the sphere crossed $u_y = 0$ when the periodic state was reached, $u_x(u_y = 0)$ has been compared. The error was calculated as

$$\begin{aligned} \text{error}_x &= \frac{u_{x,\text{strong coupling}}(u_y = 0) - u_{x,\beta}(u_y = 0)}{u_{x,\text{strong coupling}}(u_y = 0)} \\ \text{error}_y &= \frac{u_{y,max,\text{strong coupling}} - u_{x,max,\beta}}{u_{y,max,\text{strong coupling}}} \end{aligned} \tag{4.21}$$

and the result can be seen in figure 4.29. As expected, the offset in displacement increases as β decreases. For this particular case the offset of the trajectory of the center of the cylinder, shown in figure 4.29a, becomes large when β has decreased to 0.01. For $\beta = 0.033$ the offset of the trajectory of the cylinder is still within the difference that has been obtained by previous work (compare to figure 4.15). Both error_x and error_y defined in the equation above and shown in figure 4.29b decreases as β increases in a similar manner.

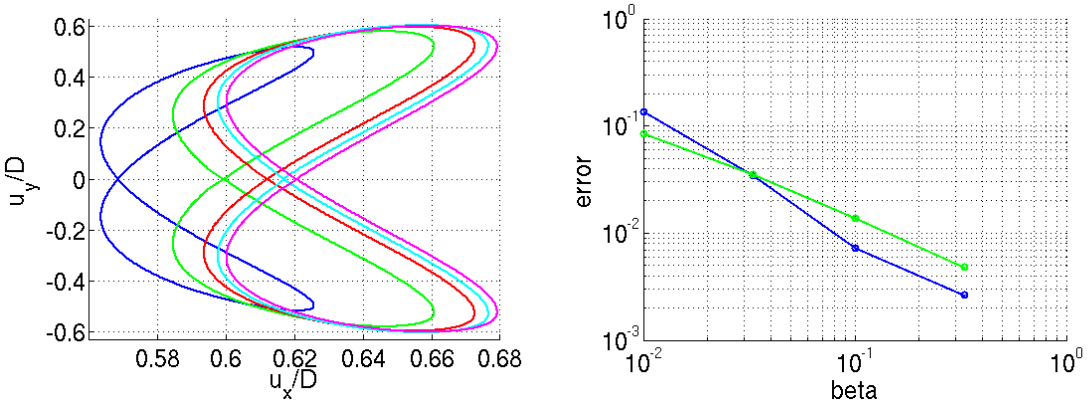

(a) Trajectory of the center of the cylinder. Comparison between force smoothing method with $\beta = 0.01$ (—), $\beta = 0.033$ (—), $\beta = 0.1$ (—), $\beta = 0.33$ (—) and strong coupling method (—)

(b) Error in amplitude of oscillations (—) and x-position, u_x, where the center of the sphere crosses $u_y = 0$ (—) when the periodic state is reached at different β.

Figure 4.29: *Accuracy of force smoothing method while solving the motion of an elastically mounted cylinder with* $\rho = 4/\pi$.

Lets study the difference in the force calculated by the fluid and the force seen by the structure. In figure 4.30 the force coefficients are shown for the solution when using the force smoothing method with $\beta = 0.1$ ($\rho = 0.1$). The amplitude of the white noise in the force seen by the structure has been drastically reduced while still preserving a good agreement with the solution obtained with the strong coupling method.

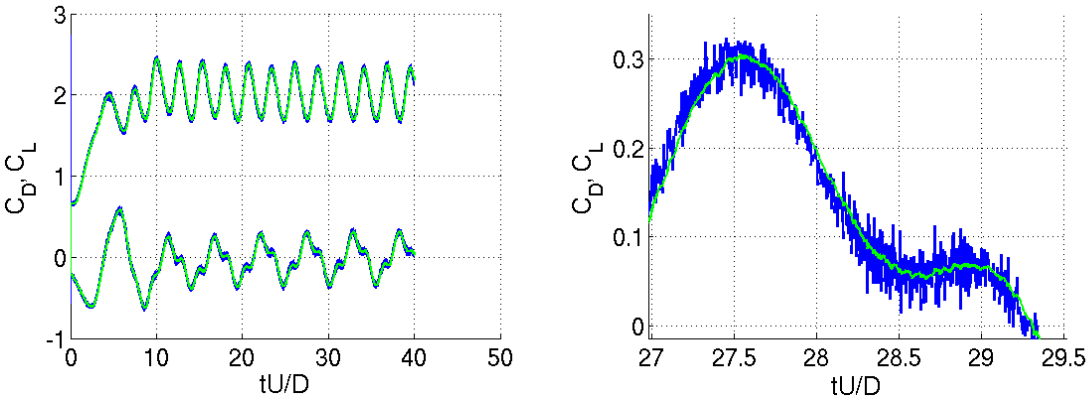

Figure 4.30: *Force coefficients plotted over time to the left and zoom to the right of an elastically mounted cylinder with* $\rho = 4/\pi$. *Force predictor method with* $\beta = 0.1$. *Force coefficient calculated by the fluid (—) and force coefficient seen by the structure (—).*

It has been established that the method produces a solution with good agreement to the solution produced by using the strong coupling method, if β is not to small. The next subject of interest is the stability of the method. Lets recall that setting $\beta = 1$

corresponds to the explicit coupling method, which has already been investigated and the stability limit of the solid-to-fluid density ratio were found to be $\rho = 0.46$. The force smoothing method with $\beta = 0.33$ was stable down to a density ratio of $\rho = 0.17$ and the results are presented and compared with the strong coupling method in figure 4.31. The agreement between the displacement and dynamic behaviour obtained by using the two different methods is excellent.

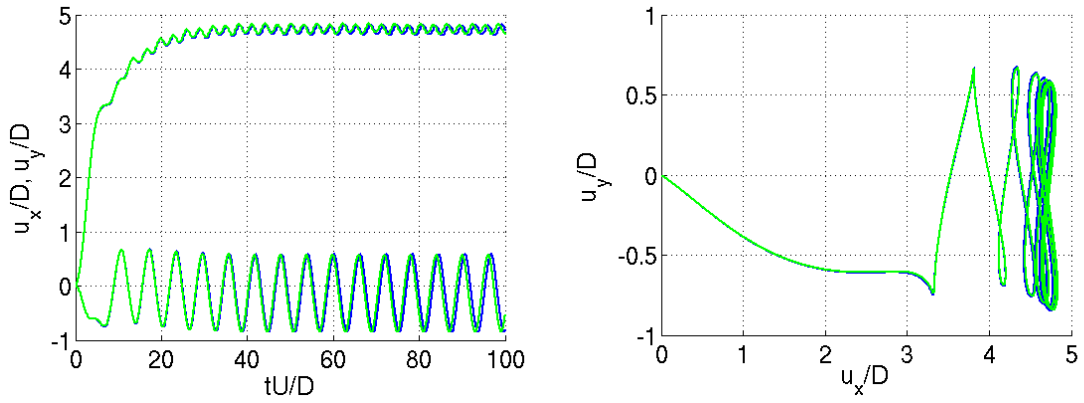

Figure 4.31: *Displacement in both x- and y-direction to the left and trajectories to the right of an elastically mounted cylinder with $\rho = 0.17$. Comparison between the force smoothing method (—) with $\beta = 0.33$ and the strong coupling method (—).*

In figure 4.32 the force coefficients calculated by the fluid solver is shown together with the force seen by the structure when using the force smoothing method and compared to the force coefficient obtained with the strong coupling method.

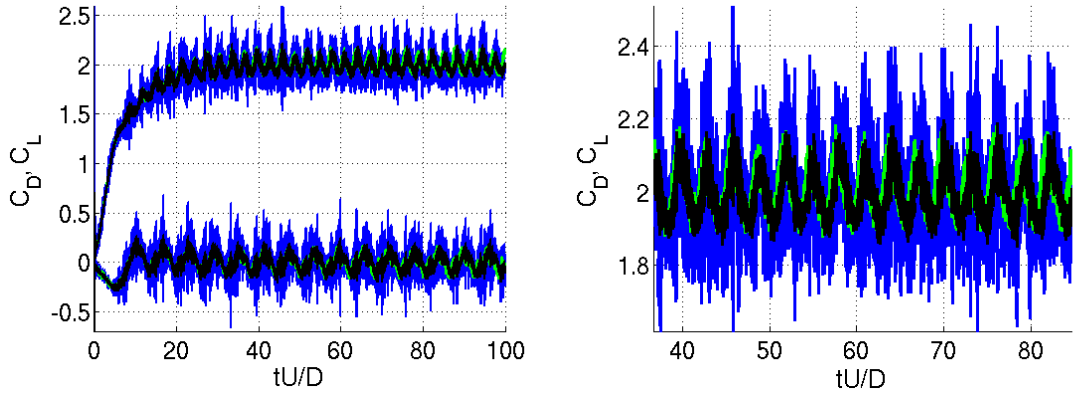

Figure 4.32: *Force coefficients plotted over time to the left and zoom to the right of an elastically mounted cylinder with $\rho = 0.17$. Comparison between the force smoothing method with $\beta = 0.33$, force coefficients calculated by fluid solver (—) and force coefficients seen by the structure (—), and the strong coupling method (—).*

The amplitude of the white noise of the force calculated by the fluid solver has increased compared to the strong coupling method. But by studying the filtered force

signal, seen by the structure, the white noise has decreased to approximately the same amplitude. The agreement between the force coefficient seen by the structure when using the force smoothing method and the strong coupling method is in good agreement. At the solid-to-fluid density ratio the strong coupling needed an average of 4.9 iterations in order to reach convergence. Meaning that the computational cost has decreased by a factor of approximately five by using the force smoothing method.

As expected, decreasing β further yielded even better stability. Setting $\beta = 0.1$ yielded a stable solution down to a solid-to-fluid density ratio of $\rho = 0.06$ and the result is presented in figure 4.33. The same phenomenon as for $\beta = 0.33$ can be observed. The amplitude of the white noise in the forces calculated by the fluid has increased compared to the strong coupling method but regarding the filtered forces, seen by the structure, the white noise has a similar amplitude and are in good agreement with the forces obtained by using the strong coupling method. At this density ratio an average of 6.2 iterations was needed in order to reach convergence, meaning that the computational cost has decreased with a factor of approximately six by using the force smoothing method.

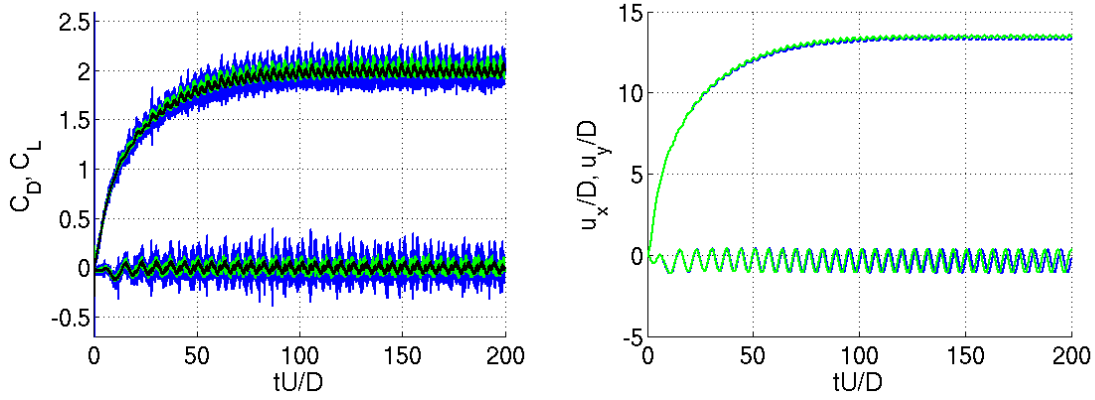

Figure 4.33: *Force coefficients plotted over time to the left and displacement to the right of an elastically mounted cylinder with $\rho = 0.06$. Comparison between the force smoothing method with $\beta = 0.1$, force coefficients calculated by fluid solver (—) and force coefficients seen by the structure (—), and the strong coupling method (—).*

Decreasing β to $\beta = 0.033$ yielded a stability limit of a solid-to-fluid density of $\rho = 0.02$. But at this density ratio, the displacement in $x-$direction becomes larger than the distance between the initial position of the sphere to the outlet. Meaning that the stability at this β is better than the benchmarking case is designed for. The same goes for decreasing β further.

4.2.6 Summary

The accuracy and stability of different weak coupling methods has been investigated using a case where a cylinder is elastically mounted in a laminar flow. Firstly a time step and a mesh dependency study was performed using the existing strong coupling method. The results showed good agreement with previous study and the spatial and

temporal convergence ratio approached second order accuracy. The explicit coupling method showed good agreement with the strong coupling method. The interface predicting method did not improve the stability compared to the explicit coupling and caused an offset in displacement compared to the strong coupling method. The force predicting method increased stability issues compared to the explicit coupling due to the extrapolation of forces which increased the white noise that occurs in the force signal. The force smoothing method showed promising results. The accuracy depended on the choice of β, if β is chosen to $\beta = 1$ the method becomes identical with the explicit coupling method and if β is decreased too much an offset in displacement can be observed. Decreasing β increased the stability of the method.

The smallest density ratio where a solution could be obtained was well below those that has been achieved in previous work, and even lower than the lowest density ratio that could be investigated by using this benchmark case. Kim and co-workers[33] obtained a stable solution down to a solid-to-fluid density ratio of $\rho = 0.21$ by using a weak coupling algorithm and Yang et al. [56] were able to obtain a stable solution down to $\rho = 1.08$. The lowest density ratio where a stable solution could be obtained using the force smoothing method in this thesis were $\rho < 0.02$.

In table 4.4 a summation of the simulated cases is given and compared to results obtained in [33]. The accuracy is given as the $x-$position, u_x, of where $u_y = 0$ and an x indicates that a stable solution could not be achieved. The agreement in displacement with those of the previous study is excellent.

Table 4.4: *Summation of stability and accuracy in displacement in $x-$direction of an elastically mounted rigid cylinder. The values in the table represents the $x-$position where the center of the cylinder passes the $x-axis$, $(u_x(u_y = 0))$, and x indicates that a stable solution could not be produced. For reference the results from a previous study is also given to the right.*

		Weak couplings										Strong coupling	[33]
		Explicit	Interface Predicting			Force Predicting			Force Smoothing				
			Equation			β			β				
			3.10	3.11	3.12	1	0.33	0.1	0.33	0.1	0.033		
	1.5					0.616							
	1.4					x	0.666						
	1.3					x	x						
	$4/\pi$	0.618	0.540	0.540	0.540	x	x	0.741	0.617	0.611	0.598	0.620	0.622
	1.1					x	x	0.875					
	1.0					x	x	x					
	0.7					x	x	x				1.14	1.14
	0.5					x	x	x				1.60	1.61
ρ	0.46	1.73	1.48	1.48	1.48	x	x	x	1.73	1.72	1.70	1.74	
	0.45	x	x	x	x	x	x	x					
	0.4	x	x	x	x	x	x	x				2.00	2.02
	0.21	x	x	x	x	x	x	x					2.87
	0.20	x	x	x	x	x	x	x					x
	0.17	x	x	x	x	x	x	x	4.70	4.68		4.71	x
	0.17	x	x	x	x	x	x	x	x				x
	0.06	x	x	x	x	x	x	x	x	13.3		13.4	x
	0.05	x	x	x	x	x	x	x	x	x			x
	0.02	x	x	x	x	x	x	x	x	x	>30	>30	x
	0.01	x	x	x	x	x	x	x	x	x	x	-	x

The number of iterations needed in order to reach convergence for the strong coupling method varied between four and six depending on the chosen density ratio. Meaning that the computational cost needed in order to solve the case decreased with a factor of between four and six when using weak coupling method instead of a strong coupling method.

In figure 4.34 the movement of the vorticity contours during one period when the periodic state is reached is shown. The vorticity behaves as expected. During one period two vortices are created and are transported down stream where the intensity of them decreases and dissipates into the mean flow.

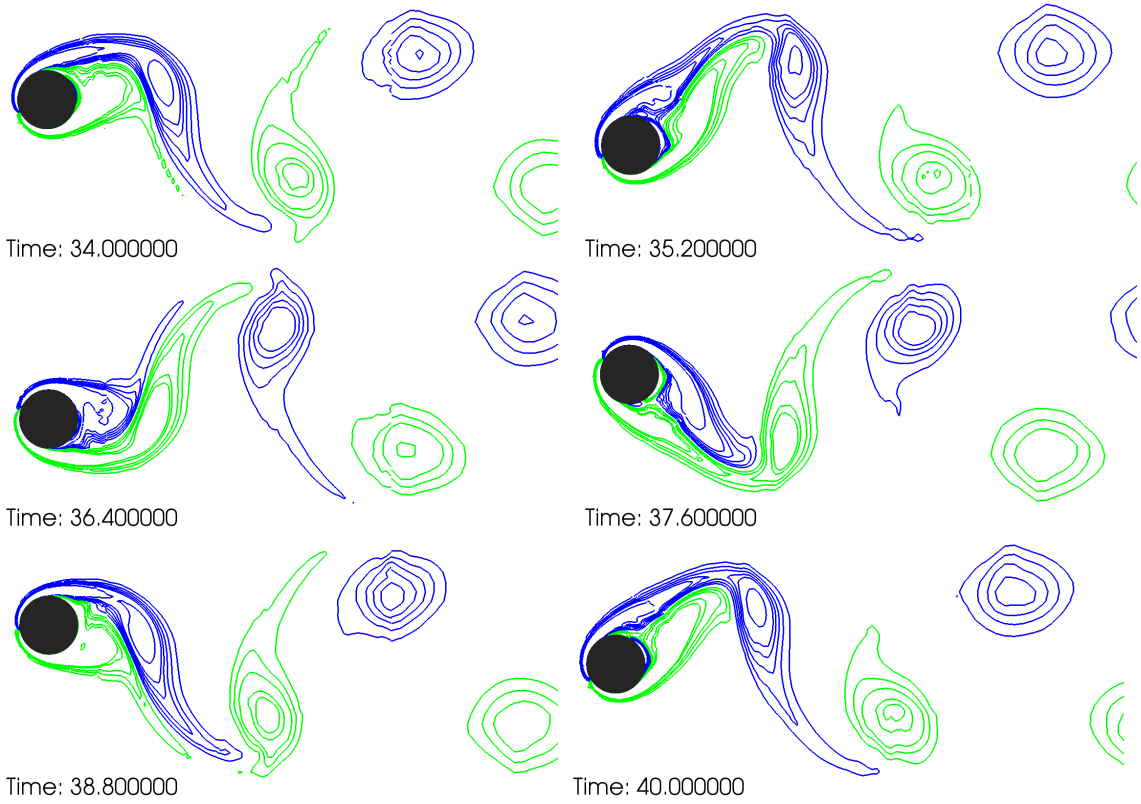

Figure 4.34: *Countours of the instantaneous vorticity of an elastically mounted cylinder with $\rho = 4/\pi$ during approximately one period. (—) indicates negative vorticity while (—) indicates positive vorticity.*

4.3 Numerical Case: Flexible Beam Attached to a Rigid Cylinder in an Incompressible Laminar Flow

So far in this thesis only cases where the structures consists of rigid bodies have been treated. It is also of interest to study fluid structure interaction where the structures consists of elastic bodies. This case consists of an elastic beam attached to a rigid cylinder in an incompressible laminar channel flow. It wwas originally proposed by Turek and Hron in [57] and has since then been used to validate and investigate the stability of fluid structure interaction solvers in a wide variety of articles [31], [58] and [33] among others.

The domain is illustrated in figure 4.35. The inlet is treated as a velocity inlet where a parabolic velocity profile is prescribed according to

$$u(t) = 1.5\bar{U}\frac{y(H-y)}{(H/2)^2}. \tag{4.22}$$

where $\bar{U}$ is the mean velocity. The boundaries at $y = 0$ and $y = H$ are treated as no-slip walls and the outlet is prescribed as a pressure outlet with zero pressure.

The size of the domain and the immersed objects are as follows:

- The domain has the length $L = 2.5$ m and height $H = 0.41$ m and the left lower corner is placed in $(x, y) = (0, 0)$.
- The rigid cylinder center is placed in $(x, y) = (0.2, 0.2)$ m and the radius is set to $r = 0.05$ m.
- The elastic bar has the length $l = 0.35$ m and the height $h = 0.02$ m.
- The point A, shown in the figure, is initially placed in $(x, y) = (0.2, 0.6)$ m.

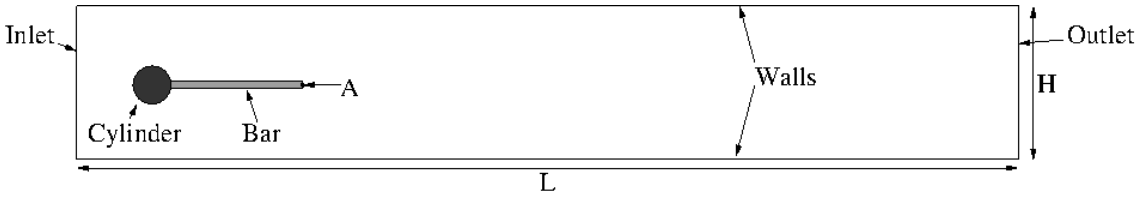

Figure 4.35: *A schematic diagram of the computational domain for an elastic beam attached to a rigid cylinder and initial shape of the structure. Note that the diagram is not to scale.*

Turek and Hron [57] proposed three cases where the inlet velocity and the stiffness of the beam is varied. The first one, called **FSI1**, resulted in a steady state solution while the two others, **FSI2** and **FSI3**, resulted in a periodic behaviour. The different parameters for the three cases are presented in figure 4.5

Table 4.5: *Used parameters for an elastic beam attached to a rigid cylinder.*

		FSI1	**FSI2**	**FSI3**
inlet mean velocity	$\bar{U}$ [m/s]	0.2	1	2
fluid density	ρ_f [10^3kg/m^3]	1	1	1
fluid viscosity	μ_f [kg/ms]	1	1	1
solid density	ρ_s [10^3kg/m^3]	1	10	1
Poission's ratio	ν_s [-]	0.4	0.4	0.4
Young's modulus	E_s [10^3Pa]	1.4	1.4	5.6

In this thesis only **FSI2** and **FSI3** has been investigated. A stable solution which were in agreement with previous studies could only be produced with the strong coupling method. Hence, a grid and time step dependency study is given and followed by some analysis and comparison with solutions obtained with the different weak coupling methods.

In order to compare the results with previous studies some quantities needs to be compared. The quantities for comparison has been chosen as

- The displacement of the point A on the structure, see figure 4.35, over time in both streamwise direction, $u_x(t)$, and vertical direction, $u_y(t)$.
- The force exerted by the fluid on the immersed body both in streamwise direction, $F_x(t)$, and vertical direction, $F_y(t)$.
- The frequency of the displacement.

In order to reassure that spatial convergence has been reached the size of the fluid cells has been varied. The smallest cell size has been $\Delta x_{min} = \Delta y_{min} = 0.004$ m, $\Delta x_{min} = \Delta y_{min} = 0.002828$ m, $\Delta x_{min} = \Delta y_{min} = 0.002$ m and $\Delta x_{min} = \Delta y_{min} = 0.01414$ for the different fluid grids. In fig 4.36 an example of one of the fluid grids is given. This particular grid has a smallest cell size of $\Delta x_{min} = \Delta y_{min} = 0.002$ m.

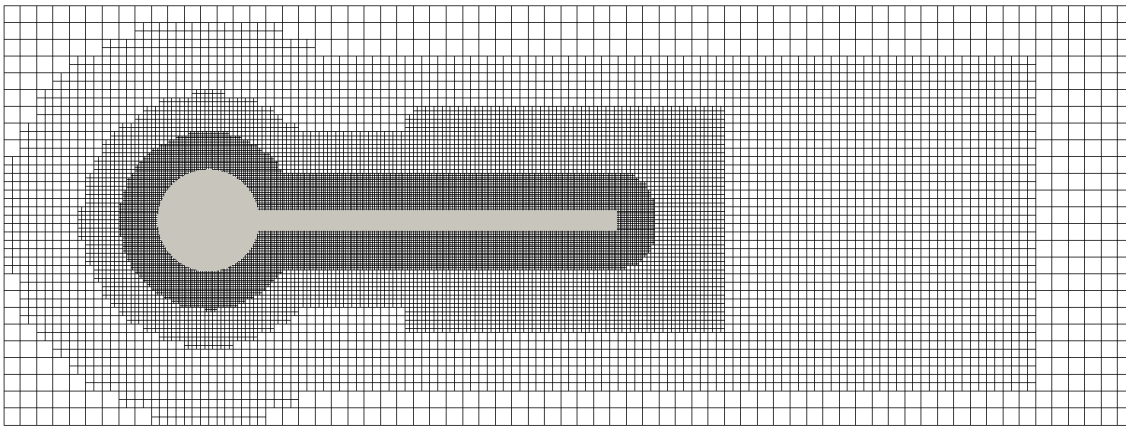

Figure 4.36: *Example of fluid grid, with $\Delta x_{min} = \Delta y_{min} = 0.002$ m, for an elastic beam attached to a rigid cylinder.*

Regarding the elastic beam the same spatial discretization has been used for all simulations. The spatial discretization consists of 446 elements and is shown in figure 4.37.

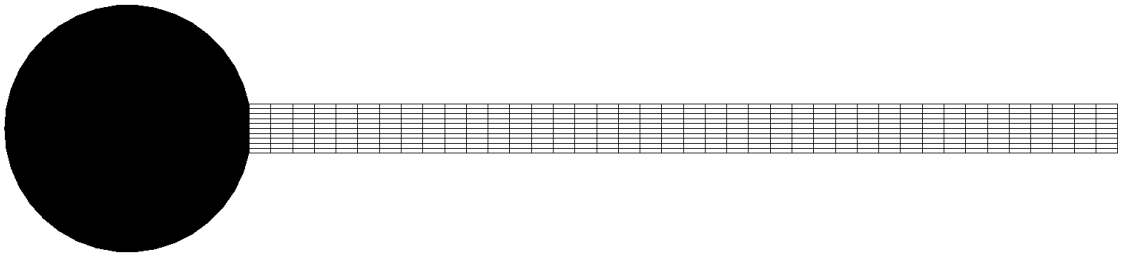

Figure 4.37: *Spatial discretization of the structure for an elastic beam attached to a rigid cylinder.*

The time step has also been varied and the different used time steps has been $\Delta t = 4$ ms, $\Delta t = 2$ ms, $\Delta t = 1$ ms and $\Delta t = 0.5$ ms.

4.3.1 Validation

In the following section the strong coupling procedure has been validated using the cases **FSI2** and **FSI3**. The convergence criteria has been set to $\varepsilon = 10^{-3}$.

4.3.1.1 FSI2

The case has been solved with three different time steps and three different grids. The time steps have been $\Delta t = 4$ ms, $\Delta t = 2$ ms and $\Delta t = 1$ ms. The results for the different time steps are shown in figure 4.38. The results are obtained with a grid which has the smallest cell $\Delta x_{min} = \Delta y_{min} = 0.002$ m. The agreement in displacement between all three time steps are good and the difference between $\Delta t = 2$ ms and $\Delta t = 1$ ms are very small. Hence, a time step of $\Delta t = 1$ ms are deemed small enough. The mean value, amplitude and frequency of the displacement is summarized in table 4.6.

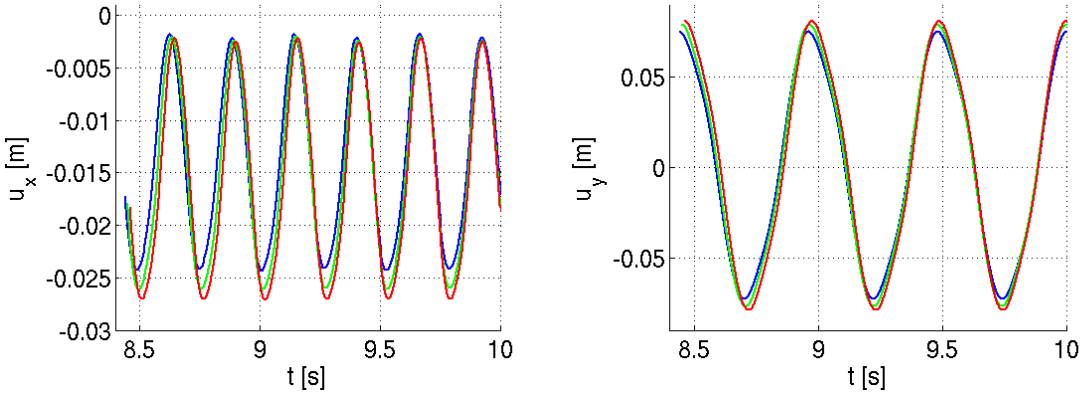

Figure 4.38: *Displacement in both x- and y-direction for point A of an elastic beam attached to a rigid cylinder (**FSI2**). Comparison between different time steps. $\Delta t = 4$ ms (—), $\Delta t = 2$ ms (—) and $\Delta t = 1$ ms (—).*

Table 4.6: *Mean value, amplitude and frequency of the displacement for point A of an elastic beam attached to a rigid cylinder (**FSI2**). Different time steps.*

		$u_x(A)$ [mm]	$u_y(A)$ [mm]
Δt [ms]	4	$-13.67 \pm 11.25[3.846]$	$1.355 \pm 73.91[1.923]$
	2	$-14.88 \pm 12.05[3.871]$	$1.198 \pm 78.00[1.935]$
	1	$-15.52 \pm 12.44[3.901]$	$1.039 \pm 80.01[1.951]$

In order to reassure that the used spatial discretization of the fluid domain was fine enough the problem was solved with three different fluid grids. The cell size was varied by decreasing the size of the biggest cells and keeping all refinements, meaning that decreasing the length of one cell by two would increase the number of cells in the domain by approximately four. The three different grids had a smallest cell size of $\Delta x_{min} = \Delta y_{min} = 0.004$ m, $\Delta x_{min} = \Delta y_{min} = 0.002828$ m and $\Delta x_{min} = \Delta y_{min} = 0.002$ m and the time step used for all grids was set to $\Delta t = 1$ ms. The results are shown in figure 4.39. The grids with $\Delta x_{min} = \Delta y_{min} = 0.002828$ m and $\Delta x_{min} = \Delta y_{min} = 0.002$ m are in excellent agreement. Hence, the grid with $\Delta x_{min} = \Delta y_{min} = 0.002$ m is deemed fine enough. In table 4.7 the mean value, amplitude and frequency of the displacement obtained with the different grids is summarized.

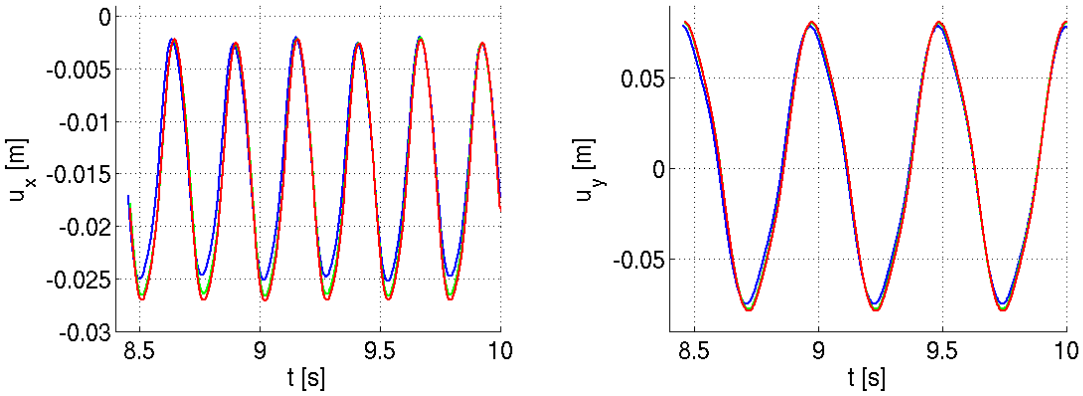

Figure 4.39: *Displacement in both x- and y-direction of point A of an elastic beam attached to a rigid cylinder (**FSI2**). Comparison between different grids.* $\Delta x_{min} = \Delta y_{min} = 0.004$ *m (—), * $\Delta x_{min} = \Delta y_{min} = 0.002828$ *m (—) and* $\Delta x_{min} = \Delta y_{min} = 0.002$ *m (—).*

Table 4.7: *Mean value, amplitude and frequency of the displacement for point A of an elastic beam attached to a rigid cylinder (**FSI2**). Different fluid grids.*

		$u_x(A)$ [mm]	$u_y(A)$ [mm]
$\Delta x_{min} = \Delta y_{min}$ [m]	0.004	$-14.32 \pm 11.64[3.881]$	$1.891 \pm 76.85[1.940]$
	0.002828	$-15.23 \pm 12.29[3.904]$	$1.440 \pm 79.21[1.952]$
	0.002	$-15.52 \pm 12.44[3.901]$	$1.039 \pm 80.01[1.951]$

It is shown that by using a time step of $\Delta t = 1$ ms and the spatial discretization where the smallest cell has a size of $\Delta x_{min} = \Delta y_{min} = 0.002$ m temporal and spatial convergence is ensured.

In figure 4.40 the displacement is compared to the one obtained in [57]. The agreement between the two are excellent.

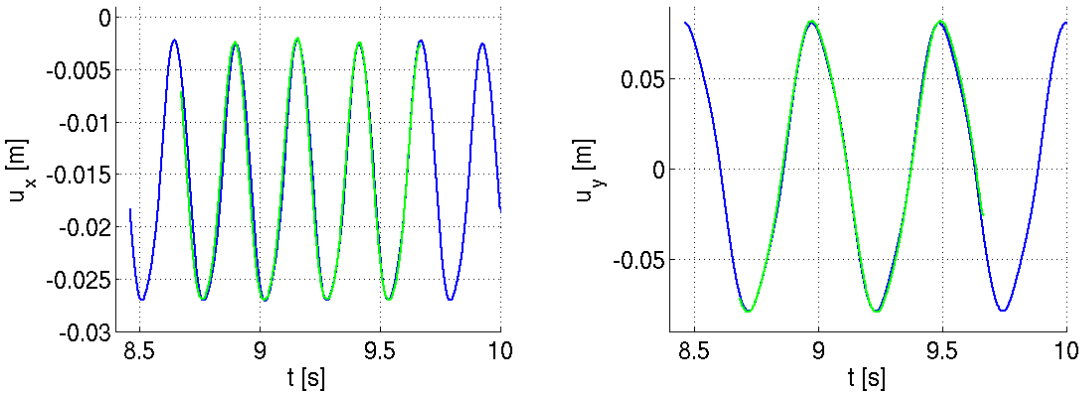

Figure 4.40: *Displacement in both x- and y-direction for point A of an elastic beam attached to a rigid cylinder (**FSI2**). Comparison between obtained results with* $\Delta x_{min} = \Delta y_{min} = 0.002$ *m and* $\Delta t = 1$ *ms (—) and results from [57] (—).*

In figure 4.41 the drag force and the lift force is shown and compared to the one obtained in [57]. The overall behaviour is similar for both forces, but a small increase in mean value of the drag force has occurred. The, previously discussed, white noise in the force signal can still be observed. The amplitude of the white noise in the lift force is slightly higher compared to the amplitude of the white noise in the drag force.

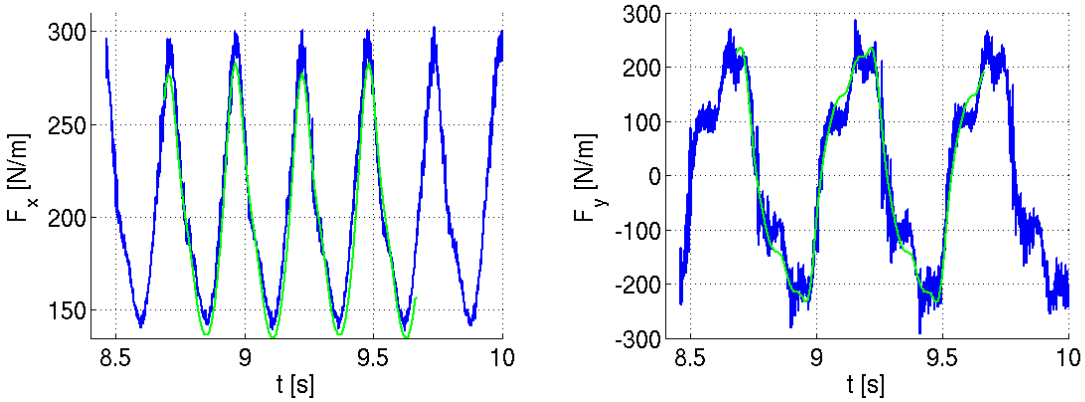

Figure 4.41: *Drag and lift force of an elastic beam attached to a rigid cylinder (**FSI2**). Comparison between obtained results with $\Delta x_{min} = \Delta y_{min} = 0.002$ m and $\Delta t = 1$ ms (—) and results from [57] (—).*

The vorticity contours during one period is shown in figure 4.42. Two vortices are created in each period and the vorticity behaves as expected.

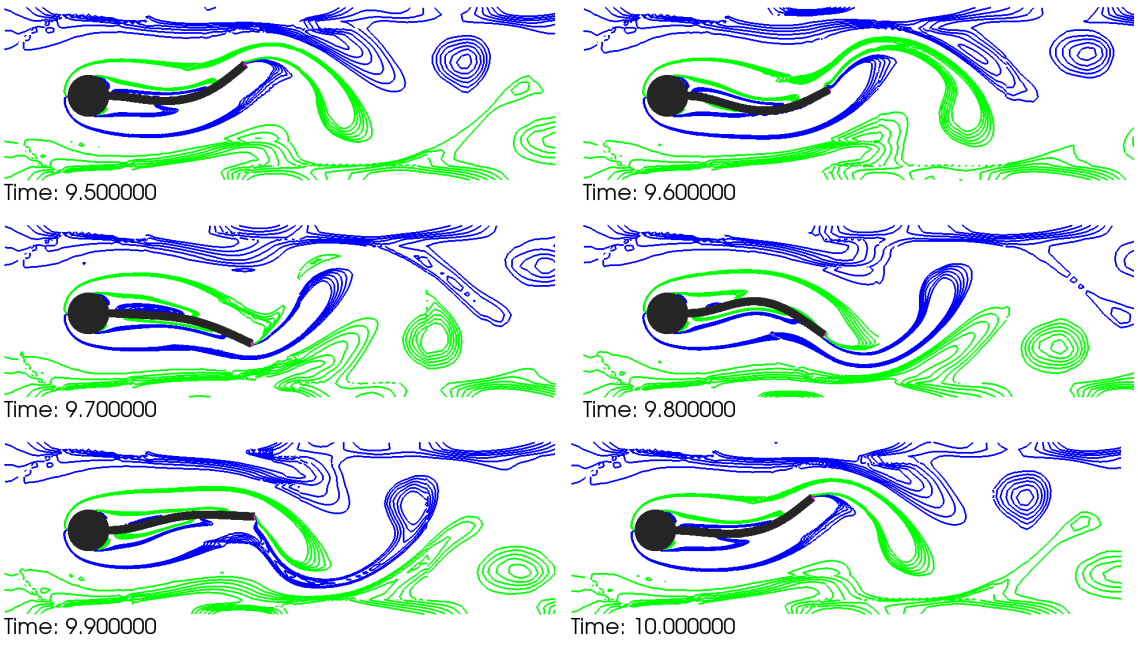

Figure 4.42: *Countours of the instantaneous vorticity of an elastic beam attached to a rigid cylinder during approximately one period(**FSI2**). (—) indicates negative vorticity while (—) indicates positive vorticity.*

In contrast to the vorticity around the elastically mounted sphere, shown in figure 4.34, vorticity occurs along the upper and the lower boundaries. This is due to the no slip boundary conditions along these boundaries, which is different in the other case.

In average 11 coupling iterations were needed in order to reach convergence. Meaning that by successfully applying a weak coupling method to solve this case the computational cost would decrease with a factor of 11.

4.3.1.2 FSI3

A similar time step and grid dependency study has been made for the **FSI3** case as for the **FSI2** case. Firstly the case was simulated with three different time steps at the same grid, with a smallest cell size of $\Delta x_{min} = \Delta y_{min} = 0.002$ m. The different time steps were $\Delta t = 2$ ms, $\Delta t = 1$ ms and $\Delta t = 0.5$ ms and the obtained displacement for point A is shown in figure 4.43. An offset in the displacements occurs with the longest time step, $\Delta t = 2$ ms, while the two shorter ones, $\Delta t = 1$ ms and $\Delta t = 0.5$ ms, are in excellent agreement. In table 4.8 the mean value, amplitude and frequency of the displacements obtained with the different time steps are summarized.

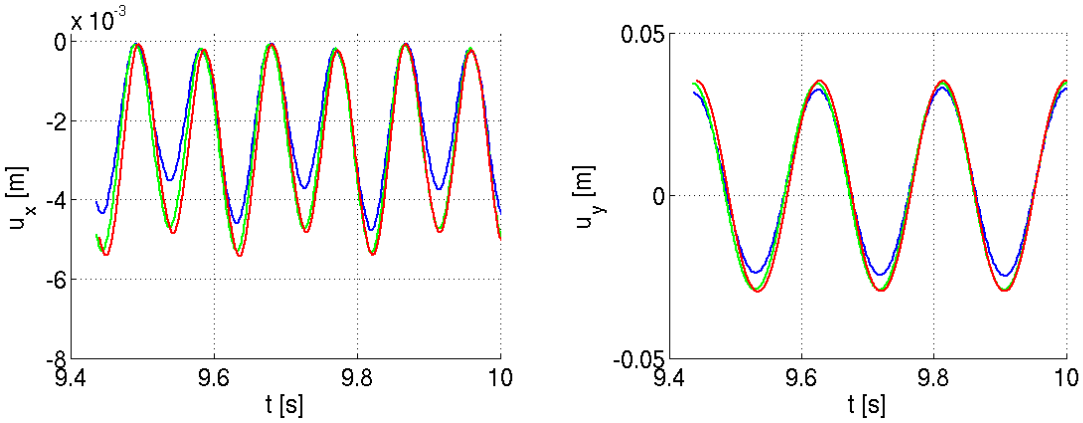

Figure 4.43: *Displacement in both x- and y-direction for point A of an elastic beam attached to a rigid cylinder (**FSI3**). Comparison between different time steps. $\Delta t = 2$ ms (—), $\Delta t = 1$ ms (—) and $\Delta t = 0.5$ ms (—).*

Table 4.8: *Mean value, amplitude and frequency of the displacement for point A of an elastic beam attached to a rigid cylinder (**FSI3**). Different time steps.*

		$u_x(A)$ [mm]	$u_y(A)$ [mm]
Δt [ms]	2	$-2.115 \pm 2.355[10.64]$	$4.201 \pm 28.86[5.319]$
	1	$-2.565 \pm 2.623[10.64]$	$2.744 \pm 31.72[5.319]$
	0.55	$-2.64 \pm 2.677[10.73]$	$2.847 \pm 32.4[5.367]$

For the grid dependency study three different grids were used with a smallest cell size of $\Delta x_{min} = \Delta y_{min} = 0.002828$ m, $\Delta x_{min} = \Delta y_{min} = 0.002$ m and $\Delta x_{min} = \Delta y_{min} = 0.001414$ m. The time step was kept as $\Delta t = 0.5$ ms for all three grids.

The results are shown in figure 4.44. The obtained displacement while using the two finer grids, $\Delta x_{min} = \Delta y_{min} = 0.002$ m and $\Delta x_{min} = \Delta y_{min} = 0.001414$ m, are in excellent agreement. In table 4.9 the mean value, displacement and frequency of the displacements are summarized.

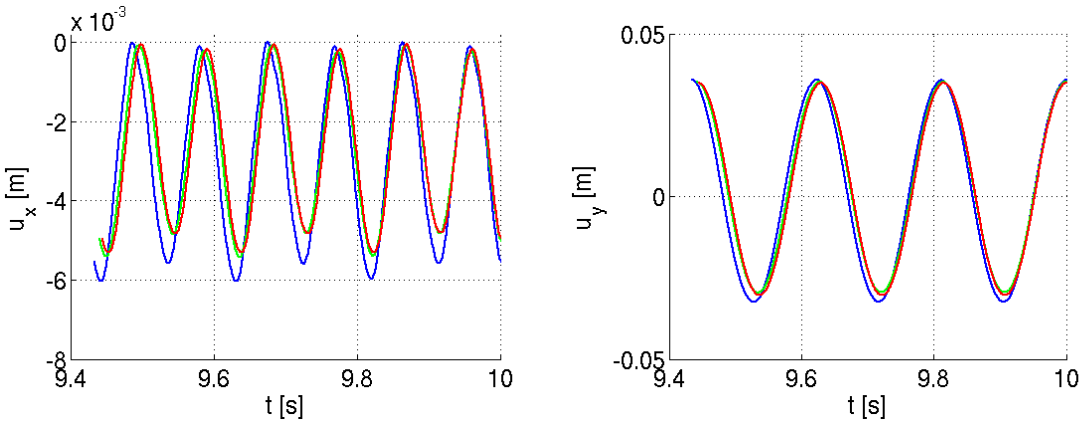

Figure 4.44: *Displacement in both x- and y-direction for point A of an elastic beam attached to a rigid cylinder (**FSI3**). Comparison between different grids.* $\Delta x_{min} = \Delta y_{min} = 0.002828$ *m (—), * $\Delta x_{min} = \Delta y_{min} = 0.002$ *m (—) and* $\Delta x_{min} = \Delta y_{min} = 0.001414$ *m (—).*

Table 4.9: *Mean value, amplitude and frequency of the displacement for point A of an elastic beam attached to a rigid cylinder (**FSI3**). Different fluid grids.*

		$u_x(A)$ [mm]	$u_y(A)$ [mm]
$\Delta x_{min} = \Delta y_{min}$ [m]	0.002828	$-2.953 \pm 3.02[10.59]$	$1.654 \pm 34.14[5.296]$
	0.002	$-2.64 \pm 2.677[10.73]$	$2.847 \pm 32.4[5.367]$
	0.001414	$-2.648 \pm 2.63[10.8]$	$2.259 \pm 32.62[5.401]$

In figure 4.45 the obtained displacement is compared to the the one obtained in [57]. A small offset in displacement can be observed, but the two are still in good agreement. For every time u_y reaches a local maximum or minimum value u_x reaches a local maximum or minimum value two times. In the obtained solution the difference between these two local minimum values for u_x is bigger compared to the the displacement obtained in [57]. The reason for this difference has not been investigated in the thesis.

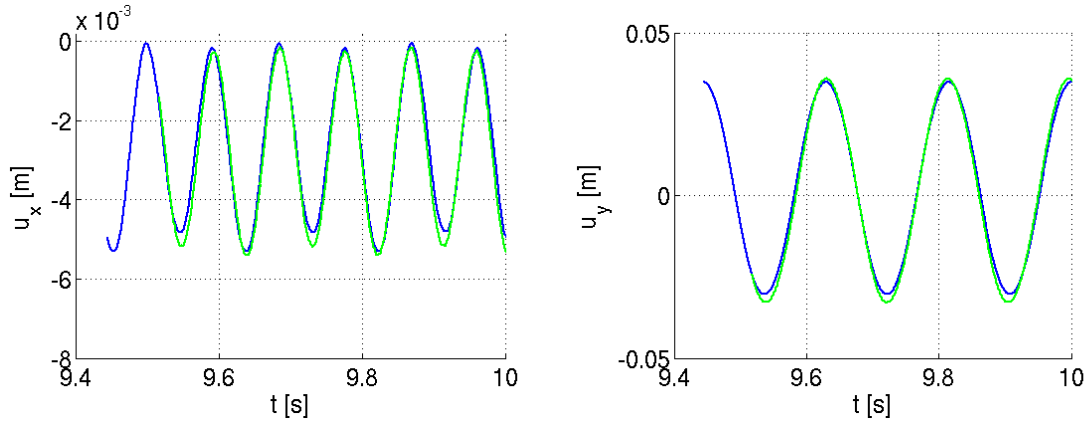

Figure 4.45: *Displacement in both x- and y-direction for point A of an elastic beam attached to a rigid cylinder (**FSI3**). Comparison between obtained results with* $\Delta x_{min} = \Delta y_{min} = 0.001414$ *m and* $\Delta t = 0.5$ *ms (—) and results from [57] (—).*

In figure 4.46 the obtained fluid forces are compared to those from [57]. A white noise of a similar amplitude as for the forces obtained for the **FSI2** case can be seen. Aside from this the behaviour of the lift forces, F_y, are in good agreement. The drag force, F_x, has a similar behaviour, amplitude and frequency but the mean value has an offset of approximately 20 N compared to the drag force in [57].

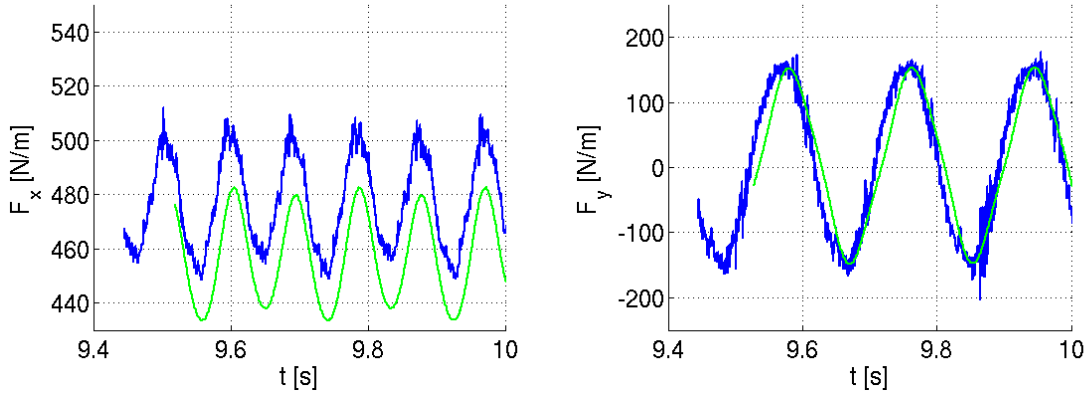

Figure 4.46: *Drag and lift force of an elastic beam attached to a rigid cylinder (**FSI3**). Comparison between obtained results with* $\Delta x_{min} = \Delta y_{min} = 0.001414$ *m and* $\Delta t = 0.5$ *ms (—) and results from [57] (—).*

In figure 4.47 the vorticity countours are shown during one period. As for the **FSI2** two vortices are created in each period. But the distance to where the shedding occurs from the structure is further down stream. This is due to the increased velocity and decreased displacement, which is caused by the increased stiffness.

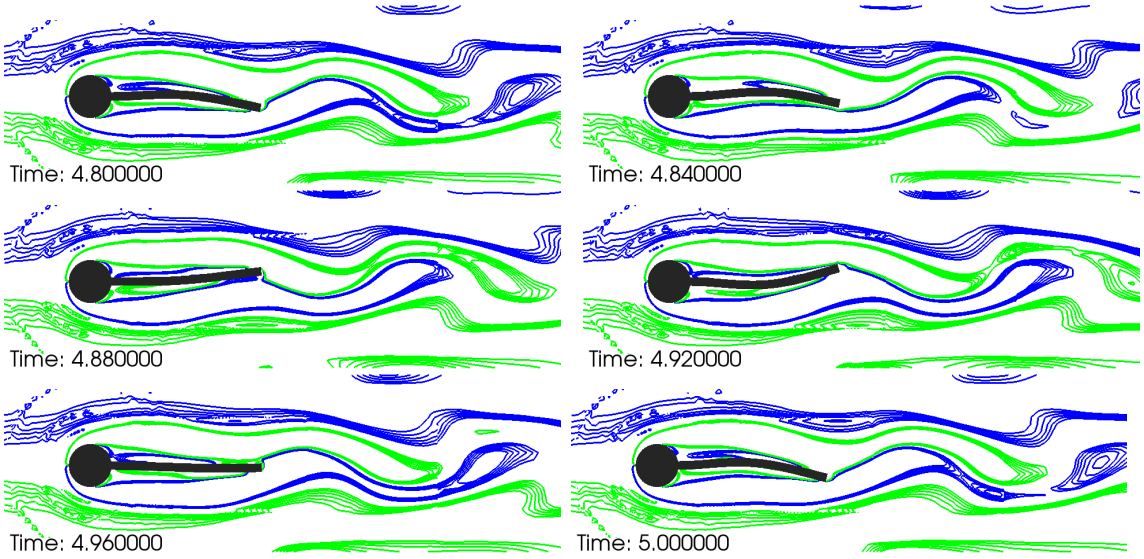

Figure 4.47: *Countours of the instantaneous vorticity of an elastic beam attached to a rigid cylinder during approximately one period (**FSI3**). (—) indicates negative vorticity while (—) indicates positive vorticity.*

In average 21 coupling iterations were needed in order to reach convergence. Meaning that successfully solving this case with a weak coupling method would decrease the computational cost with a factor of 21.

4.3.2 Force Smoothing Method

The force smoothing method presented in algorithm 4 was the only weak coupling able to produce a stable solution for the elastic beam attached to a rigid cylinder. But in order to achieve a stable solution a $\beta = 0.0004$ was needed. The solution has been calculated for $\beta = 0.0004$ and $\beta = 0.0002$ and the obtained displacement in $y-$direction is compared to the one obtained with the strong coupling in figure 4.48. Setting β to such a small value creates an big offset in both displacement and frequency. Recall that the domain only stretches from $y = -0.2$ to $y = 0.21$ meaning that the amplitude of the oscillations are even bigger than the domain itself, which is nonphysical. As β decreases the force smoothing method should be less capable of capturing high frequencies. This is confirmed in figure 4.48, where the frequency of the obtained oscillations are bigger with $\beta = 0.0004$ compared to $\beta = 0.0002$. The frequency of the displacement in $y-$direction was calculated to 1.951 Hz, 1.182 Hz and 1.1215Hz with the strong coupling method and the force smoothing method with $\beta = 0.0004$ and $\beta = 0.0002$, respectively. Meaning that the frequency was captured with a deviation of 40 %. This was not possible with the explicit coupling method and might be useful in some industrial applications.

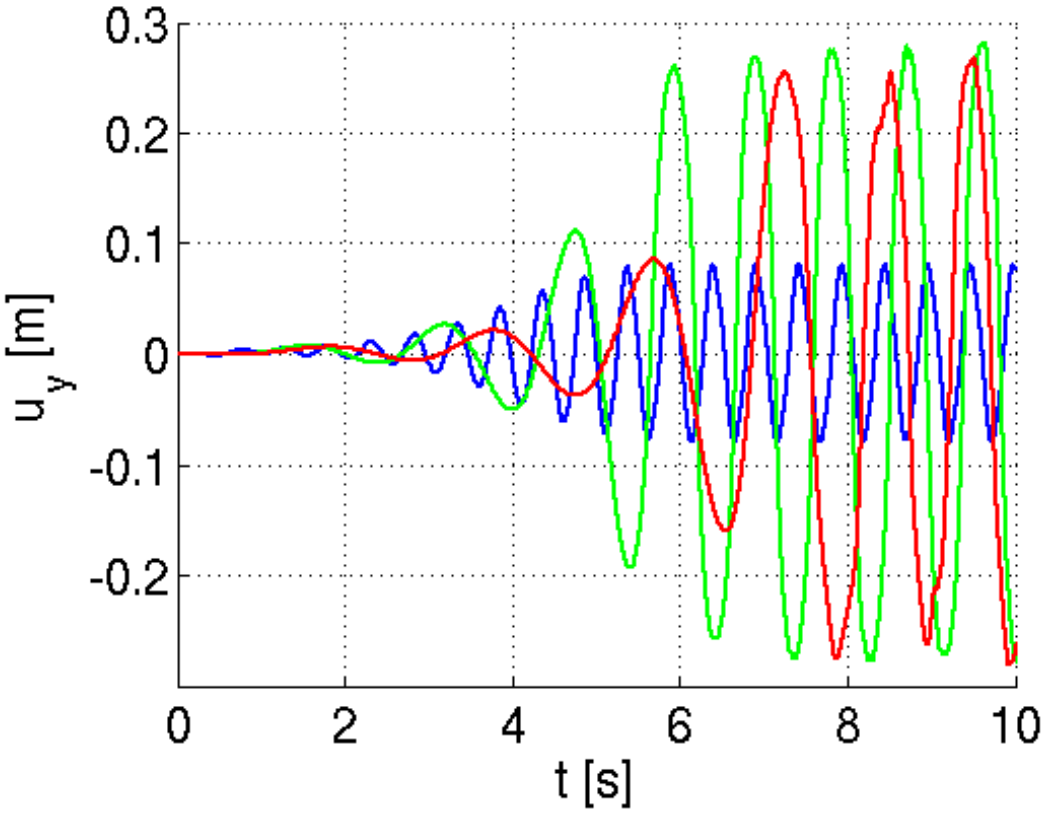

Figure 4.48: *Displacement in y-direction for point A of an elastic beam attached to a rigid cylinder (**FSI2**). Comparison between the strong coupling method (—) and the force smoothing method with $\beta = 0.0004$ (—) and $\beta = 0.0002$ (—).*

4.3.3 New Ideas for Increased Stability

When studying the reason for the severe stability issues when solving the elastic beam attached to a rigid cylinder using weak coupling methods it was found that oscillating velocities of the structural interface caused big problems. Hence, a filtering of the velocities of the interface was tested in order to investigate the effect on the stability. The method is basically equivalent with the interface predicting method presented in algorithm 2 and the only difference is how the acceleration, velocity and position of the interface is predicted. The prediction is done according to

$$\begin{aligned} \tilde{\ddot{\mathbf{x}}}^n &= \ddot{\mathbf{x}}^{n-1}, \\ \tilde{\dot{\mathbf{x}}}^n &= \beta \dot{\mathbf{x}}^{n-1} + (1-\beta)\tilde{\dot{\mathbf{x}}}^{n-1}, \\ \tilde{\mathbf{x}}^n &= \mathbf{x}^{n-1} \end{aligned} \tag{4.23}$$

In order to achieve a stable solution a β of 0.06 were needed. The obtained displacement by using this prediction with $\beta = 0.06$ and $\beta = 0.05$ is compared to the obtained displacement by using the strong coupling method is shown in figure 4.49.

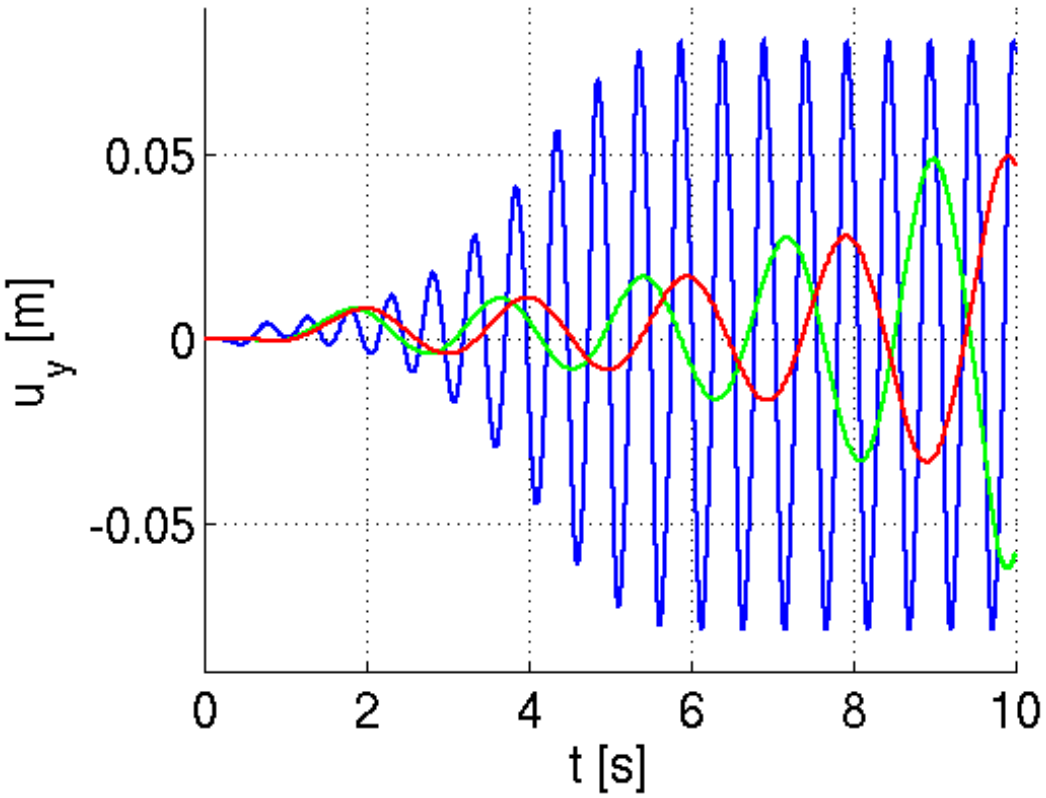

Figure 4.49: *Displacement in y-direction for point A of an elastic beam attached to a rigid cylinder (**FSI2**). Comparison between the strong coupling method (—) and the interface predicting method with the interface predicted according to equation 4.23 $\beta = 0.06$ (—) and $\beta = 0.05$ (—).*

With this method it also exist a displacement in both frequency and displacement. But it would be of interest to further investigate what could be done about the velocity of the interface in order to increase the stability of weak coupling algorithms.

4.3.4 Summary

The strong coupling method has been validated using the two case **FSI2** and **FSI3**. Both temporal and spatial convergence was achieved for both cases. The number of coupling iterations needed in order to reach convergence were found to be 11 in average for **FSI2** and 21 for **FSI3**. The mean value, amplitude and frequency are summarized and compared to results from previous studies in table 4.10. The only one of the proposed weak coupling methods that was able to produce a stable solution was the force smoothing method. But a very small β was needed, which caused a big offset in both amplitude and frequency of the displacement compared to the displacement obtained by using the strong coupling method. A small analysis of the impact of filtering the velocity in a weak coupling method of the interface was given, which yielded an increase in stability but decreased the accuracy in both amplitudes and frequency of the displacement.

Table 4.10: *Summation of mean value, amplitude and frequency of the displacement for point A of an elastic beam attached to a rigid cylinder (**FSI2** and **FSI3**) and comparison with previous studies.*

		$u_x(A)$ [mm]	$u_y(A)$ [mm]
FSI2	Obtained results	$-15.52 \pm 12.44[3.901]$	$1.039 \pm 80.01[1.951]$
	Turek and Hron[57]	$14.58 \pm 12.44[3.8]$	$1.23 \pm 80.6[2.0]$
	He and co-workers[31]	$-13.56 \pm 11.96[-]$	$1.2 \pm 77.5[-]$
	Deegroote and co-workers[58]	$-14.07 \pm 12.37[3.7]$	$1.18 \pm 76.5[1.9]$
FSI3	Obtained results	$-2.648 \pm 2.63[10.8]$	$2.259 \pm 32.62[5.401]$
	Turek and Hron[57]	$-2.69 \pm 2.53[10.9]$	$1.48 \pm 34.38[5.3]$
	He and co-workers[31]	$-2.40 \pm 2.30[-]$	$1.35 \pm 32.33[-]$

5
Conclusion and Future Work

In this section the conclusions drawn from the present work is presented and what possible future work could consist of is proposed.

5.1 Conclusion

The present work has consisted of a literature review, implementation of known coupling methods and one new method in an existing frame work for fluid structure interaction. An accuracy and stability analysis of existing coupling methods and the implemented ones was performed.

In the literature review three different weak coupling methods were found, which has been called the explicit coupling method, the interface coupling method and the force predictor method in this thesis. Beyond these a fourth one has been developed in the thesis called the force smoothing method. The coupling methods has been investigated and compared to a strong coupling method, which enforces equilibrium at each time step.

Three cases has been investigated. The first one consisted of a rigid sphere attached to an undamped spring in Stokes flow, the second one consisted of a rigid cylinder attached to a damped spring in a laminar flow and the last one consisted of an elastic bar attached to a rigid cylinder in a laminar flow. All coupling methods have been tested on all cases.

With the first case, a quite limited analysis of the accuracy was conducted. The strong coupling method showed good agreement with the analytic solution. All three of the explicit coupling method, the force predicting method and the force smoothing method showed a similar degree of agreement with the strong coupling method while the interface predictor method showed excellent agreement with the strong coupling method. By using a weak coupling method the computational power was decreased with a factor of approximately four.

In the second case, the strong coupling method showed second-order accuracy for both temporal and spatial convergence rate and the result was in excellent agreement with previous studies. The explicit coupling method showed excellent agreement with the strong coupling method and was stable down to a solid-to-fluid density ratio of $\rho = 0.46$. The interface predictor method and the force predictor method both

caused a considerable offset in both fluid forces and displacement. The interface predictor method had the same stability limit as for the explicit coupling method while the force predictor method caused instabilities at a considerable higher solid-to-fluid density ratio. The force smoothing method showed good agreement with the strong coupling method as long as the filtering variable, β, was not chosen to a too small value. The stability of the force smoothing method was superior compared to the other weak coupling methods. At $\beta = 0.1$ the force smoothing method was stable down to a density ratio of $\rho = 0.06$ and the displacement of the solution deviated with less than 1% from the solution obtained with the strong coupling method. At $\beta = 0.033$ the stability of the method exceeded the stability limit of which could be investigated with the current case. The weak coupling methods decreased the computational cost with a factor of four to six, depending on the density ratio. It should be noted that the lowest solid-to-fluid density ratio where a stable solution has been obtained by using a weak coupling method found in the literature is $\rho = 0.21$.

The only weak coupling method that was able to produce a stable solution for the third case was the force smoothing method. But in order to achieve a stable solution a $\beta = 0.0004$ was needed, which caused a considerable offset in displacement of the structure. The strong coupling method showed good agreement with previous results and both temporal and spatial convergence was reached. A small analysis and discussion of the effect on stability of filtering the velocity of the fluid-solid interface was also given.

5.2 Future Work

In future work it would be interesting to spend greater effort on investigating how stable solutions can be achieved with weak coupling methods for problems consisting of elastic bodies. In the thesis it has been showed that the stability can be enhanced by filtering the velocity of the interface, it would be interesting to perform a study how this can be done without sacrificing accuracy.

It would also be of interest to study how different filtering schemes affect the stability and accuracy for the force smoothing method. Regarding the force predicting method it would be interesting to investigate which effect different filtering and extrapolation schemes has on the stability and accuracy.

Lastly it would be interesting, and very useful, to investigate the convergence rate and stability of different strong coupling methods. In the present work the only strong coupling method has been a Gauss-Seidel method with Aitken under relaxation. In the literature there exist a wide variety of different quasi-Newton methods which has been proven to increase the convergence rate, compared to a Gauss-Seidel method, and therefore decreasing the computational cost. It has also been proven that the quasi-Newton methods has better stability compared to a Gauss-Seidel method.

Bibliography

[1] IBOFlow. http://www.iboflow.com. Accessed 31 May 2018

[2] C. Farhat, "Parallel and distributed solution of coupled nonlinear dynamic aeroelastic response," M. Papadrakakis (Ed.), Parallel solution methods in computational mechanics, John Wiley & Sons, Chichester, 1997.

[3] S.M. Rifai, Z. Johan, W.P. Wang, J.P. Grisval, T.J.R. Hughes, and R.M. Ferencz, "Multiphysics simulation of flow-induced vibrations and aeroelasticity on parallel computing platforms," Computer Methods in Applied Mechanics and Engineering, vol. 174, no. 3–4, pp. 393-417, 1999.

[4] J. Zhang, L. Guo, H. Wu, A. Zhou, D. Hu, and J. Ren, "The influence of wind shear on vibration of geometrically nonlinear wind turbine blade under fluid–structure interaction," Ocean Engineering, vol. 84, Pages 14-19, 2014.

[5] J. Arrigan, V. Pakrashi, B. Basu, and S. Nagarajaiah, "Control of flapwise vibrations in wind turbine blades using semi-active tuned mass dampers," Struct. Control Health Monit., vol. 18, pp. 840-851, 2011.

[6] J. Yang, A. Agrawal, and B. Samali, "Benchmark problem for response control of wind-excited tall buildings," J Eng. Mech., vol. 130, pp. 437–446, 2004.

[7] A. Jain, and N. Jones, "Coupled flutter and buffeting analysis of long-span bridges", J. Struct. Eng., vol. 122, pp. 716–725, 1996.

[8] P. Le Tallec, and J. Mouro, "Fluid structure interaction with large structural displacements," Computer Methods in Applied Mechanics and Engineering, vol. 190, no. 24–25, pp. 3039-3067, 2001.

[9] G. Dubini, R. Pietrabissa, and F.M. Montevecchi, "Fluid-structure interaction problems in bio-fluid mechanics: a numerical study of the motion of an isolated particle freely suspended in channel flow," Medical Engineering & Physics, vol. 17, no. 8, pp. 609-617, 1995.

[10] J. De Hart, G.W. Peters, P.J. Schreurs, and F.P. Baaijens, "A two-dimensional fluid-structure interaction model of the aortic valve," J. Biomech., vol. 33, no. 9, pp. 1079-1088, 2000.

[11] P. Sidlof, "Fluid-structure interaction in human vocal folds", ParisTech, 2007.

[12] D.J. Willis, E.R. Israeli, P.O. Persson, M. Drela, J. Peraire, S.M. Swartz, and K.S. Breuer, "A Computational Framework for Fluid Structure Interaction in Biologically Inspired Flapping Flight," 25th AIAA Appl. Aerodyn. Conf., pp. 1-22, 2007.

[13] Q. Zhu, M. Wolfgang, D. Yue, and M. Triantafyllou, "Three-dimensional flow structures and vorticity control in fish-like swimming," Journal of Fluid Mechanics, vol. 468, pp. 1-28, 2002.

[14] E. Svenning, A. Mark, and F. Edelvik, "Simulation of a highly elastic structure interacting with a two-phase flow," Journal of Mathematics in Industry, vol.4, no.1, pp. 1-11, 2014.

[15] E. Svenning *et al*, "Multiphase simulation of fiber suspension flows using immersed boundary methods," Nordic Pulp and Paper Research Journal, vol. 27, no. 2, pp. 184-191, 2012.

[16] A. Mark, "The mirroring immersed boundary method," Ph.D. thesis, Chalmers University Of Technology, Göteborg, Sweden, 2008.

[17] C. S. Peskin, "Numerical analysis of blood flow in the heart," Journal of Computational Physics, vol. 25, no. 3, pp. 220-253, 1977.

[18] M. Lai, Charles S. Peskin, "An Immersed Boundary Method with Formal Second-Order Accuracy and Reduced Numerical Viscosity," Journal of Computational Physics, vol. 160, no. 2, pp. 705-719, 2000.

[19] J. Mohd-Yusof, "Combined immersed-boundary/b-spline methods for simulations of flow in comlex geometries," Technical report, Center for Turbulence Research, Annual Research Briefs, 1997.

[20] J. Mohd-Yusof, "Development of immersed boundary methods for complex geometries," Technical report, Center for Turbulence Re-search, Annual Research Briefs, 1998.

[21] E.A. Fadlun, R. Verzicco, P. Orlandi, and J. Mohd-Yusof, "Combined Immersed-Boundary Finite-Difference Methods for Three-Dimensional Complex Flow Simulations," Journal of Computational Physics, vol. 161, no. 1, pp. 35-60, 2000.

[22] S. Kang, G. Iaccarino, and P. Moin, "Accurate and efficient immersed-boundary interpolations for viscous flows," Technical report, Center for Turbulence Research, Annual Research Brief, 2004.

[23] J. Kim, D. Kim, and H. Choi, "An Immersed-Boundary Finite-Volume Method for Simulations of Flow in Complex Geometries," Journal of Computational Physics, vol. 171, no. 1, pp. 132-150, 2001.

[24] D. Kim, and H. Choi, "Immersed boundary method for flow around an arbitrarily moving body," Journal of Computational Physics, vol. 212, no. 2, pp. 662-680, 2006.

[25] S. Majumdar, G. Iaccarino, and P. Durbin, "Rans solvers with adaptive structured boundary non-conforming grids," Technical report, Center for Turbulence Research, Annual Research Briefs, 2001.

[26] Y. Tseng, and J.H. Ferziger, "A ghost-cell immersed boundary method for flow in complex geometry," Journal of Computational Physics, vol. 192, no. 2, pp. 593-623, 2003.

[27] A. Mark, R. Rundqvist, and F. Edelvik, "Comparison between different immersed boundary conditions for simulation of complex fluid flows," Fluid Dynam. Mater. Process., vol. 7, no. 3, pp. 241–258, 2011.

[28] A. Mark, and B.G.M. van Wachem, "Derivation and validation of a novel implicit second-order accurate immersed boundary method," Journal of Computational Physics, vol. 227, no. 13, pp. 6660-6680, 2008.

[29] G. Hou, J. Wang, and A. Layton, "Numerical Methods for Fluid-Structure Interaction — A Review," Communications in Computational Physics, vol. 12. no. 2, pp. 338-377, 2012.

[30] C. Förster, W.A. Wall, and E. Ramm, "Artificial added mass instabilities in sequential staggered coupling of nonlinear structures and incompressible viscous flows," Computer Methods in Applied Mechanics and Engineering, Vol. 196, no. 7, pp. 1278-1293, 2007.

[31] L. He, K. Joshi, and D. Tafti, "Study of Fluid Structure Interaction Using Sharp Interface Immersed Boundary Method," ASME. Fluids Engineering Division Summer Meeting, vol. 1A, 2016.

[32] W.X. Huang, and H.J. Sung, "An immersed boundary method for fluid–flexible structure interaction," Computer Methods in Applied Mechanics and Engineering, vol. 198, no. 33–36, pp. 2650-2661, 2009.

[33] W. Kim, I. Lee, and H. Choi, "A weak-coupling immersed boundary method for fluid–structure interaction with low density ratio of solid to fluid," Journal of Computational Physics, vol. 359, pp. 296-311, 2018.

[34] W.G. Dettmer, and D. Perić, "A new staggered scheme for fluid–structure interaction," Int. J. Numer. Meth. Engng, vol. 93, pp. 1-22, 2013.

[35] J.V. Doormaal, and G. Raithby, "Enhancements of the SIMPLE method for predicting incompressible flows," Numer. Hear Transfer, vol. 7, pp. 147-163, 1984.

[36] C. Rhie, and W. Chow, "Numerical study of the turbulent flow past an airfoil with trailing edge separation," AIAA J1, vol. 21, pp. 1527–1532, 1983.

[37] A. Mark, E. Svenning, and F. Edelvik. "An immersed boundary method for simulation of flow with heat transfer," International Journal of Heat and Mass Transfer, vol. 56 , pp. 424-435, 2013.

[38] T. Andersson, D. Nowak, T. Johnson, A. Mark, F. Edelvik, and K. Küfer. "Multiobjective Optimization of a Heat-Sink Design Using the Sandwiching Algorithm and an Immersed Boundary Conjugate Heat Transfer Solver," ASME. J. Heat Transfer, vol. 140, no. 10, 2018.

[39] F. Svelander, G. Kettil, T. Johnson, A. Mark, A. Logg and F. Edelvik, "Robust intersection of structured hexahedral meshes and degenerate triangle meshes with volume fraction applications", Numerical Algorithms 77 (4), 1029-1068, 2018

[40] R. Rundqvist, A. Mark, F. Edelvik, and J.S. Carlson, "Modeling and simulation of viscoelastic fluids using Smoothed Particle Hydrodynamics," Fluid Dyn. Mater. Proc., vol. 7, pp. 259–278, 2011.

[41] A. Mark, R. Bohlin, D. Segerdahl, F. Edelvik, and J.S. Carlson, "Optimisation of Robotised Sealing Stations in Paint Shops by Process Simulation and Automatic Path Planning," Int. J. Manufact. Res., vol. 9, pp. 4–26, 2014.

[42] M. Svensson, A. Mark, F. Edelvik, J. Kressin, R. Bolin, D. Segerdahl, J.S. Carlson, P.J. Wahlborg and M. Sundbäck, "Process simulation and automatic path planning of adhesive joining," in Procedia CIRP, 6th CIRP Conference on Assembly Technologies and Systems (CATS), Gothenburg, vol. 44, pp. 298–303, 2016.

[43] A. A. Mark, B. Andersson, S. Tafuri, K. Engstrom, H. Söröd, F. Edelvik and J.S. Carlson, "Simulation of electrostatic rotary bell spray painting in automotive paint shops", Atomization and sprays 23 (1), 2013

[44] B. Andersson, V. Golovitchev, S. Jakobsson, A. Mark, F. Edelvik, L. Davidson and J.S. Carlson, "A Modified TAB Model for Simulation of Atomization in Rotary Bell Spray Painting," J. of Mech. Eng. and Auto., vol. 3, no. 2, pp. 54-61, 2013.

[45] B. Wettervik, T. Johnson, S. Jakobsson, A. Mark, and F. Edelvik, "A domain decomposition method for three species modeling of multi-electrode negative corona discharge – with applications to electrostatic precipitators," J. Electrost., vol. 77, pp. 139-146, 2015.

[46] T. Johnson, S. Jakobsson, B. Wettervik, B. Andersson, A. Mark, F. Edelvik, "A finite volume method for electrostatic three species negative corona discharge simulations with application to externally charged powder bells," J. Electrost., vol. 74, pp. 27-36, 2015.

[47] R. Rundqvist, A. Mark, B. Andersson, A. Ålund, F. Edelvik, S. Tafuri and J.S. Carlson, "Simulation of spray painting in automotive industry", Numerical Mathematics and Advanced Applications 2009, 771-779, 2010.

[48] F. Edelvik, A. Mark, N. Karlsson, T. Johnson, and J.S. Carlson, "Math-Based Algorithms and Software for Virtual Product Realization Implemented in Automotive Paint Shops," Springer International Publishing, Cham, Switzerland, pp. 231–251, 2017.

[49] J. Göhl, K. Markstedt, A. Mark, K. MO Håkansson, P. Gatenholm and F. Edelvik, "Simulations of 3D bioprinting: predicting bioprintability of nanofibrillar inks", Biofabrication, http://iopscience.iop.org/10.1088/1758-5090/aac872, 2018

[50] B.P. Leonard, "The ULTIMATE conservative difference scheme applied to unsteady one-dimensional advection," Computer Methods in Applied Mechanics and Engineering, vol. 88, no. 1, pp. 17-74, 1991.

[51] N. Newmark, "A method of computation for structural dynamics," ASCE J. Eng. Mech. Div., vol. 85, pp. 67-94, 1959.

[52] J. Bonet, and R. Wood, "Nonlinear Contiuum Mechanics for Finite Element Analysis," Cambridge: Cambridge University Press, 1997.

[53] B.M. Irons, and R.C. Tuck, "A version of the Aitken accelerator for computer iteration," Int. J. Numer. Meth. Engng., vol. 1, pp. 275-277, 1969.

[54] G.G. Stokes, "On the Effect of the Internal Friction of Fluids on the Motion of Pendulums," Cambridge Philos. Trans., vol. 9, pp. 8-106, 1851.

[55] H.M. Blackburn, and G.E Karniadakis, "Two-and Three-Dimensional Simulations of Vortex-Induced Vibration Of a Circular Cylinder," International Society of Offshore and Polar Engineers, 1993.

[56] J. Yang, S. Preidikman, and E. Balaras, "A strongly coupled, embedded-boundary method for fluid–structure interactions of elastically mounted rigid bodies," Journal of Fluids and Structures, vol. 24, no. 2, pp. 167-182, 2008.

[57] S. Turek and J. Hron, "Proposal for numerical benchmarking of fluid-structure interaction between an elastic object and laminar incompressible flow," In H.-

J. Bungartz and M. Schäfer, editors, Fluid-Structure Interaction: Modelling, Simulation, Optimisation, LNCSE-53. Springer, 2006.

[58] J. Degroote, R. Haelterman, S. Annerel, P. Bruggeman, and J. Vierendeels, "Performance of partitioned procedures in fluid-structure interaction," Computers and Structures, vol. 88, pp. 446-457, 2010.